Materials Today Bio 26 (2024) 101046

Contents lists available at ScienceDirect

Materials Today Bio

journal homepage: www.journals.elsevier.com/materials-today-bio

Injectable self-assembled GDF5-containing dipeptide hydrogels for enhanced tendon repair

Ming Zhang [a,b,c,d], Hao Wang [a,b,c,d], Guan-Chun Dai [a,b,c,d], Pan-Pan Lu [a,b,c,d], Yu-Cheng Gao [a,b,c,d], Mu-Ming Cao [a,b,c,d], Ying-Juan Li [e], Yun-Feng Rui [a,b,c,d,*]

[a] Department of Orthopedics, Zhongda Hospital, School of Medicine, Southeast University, Nanjing, Jiangsu, PR China
[b] School of Medicine, Southeast University, Nanjing, Jiangsu, PR China
[c] Orthopaedic Trauma Institute (OTI), Southeast University, Nanjing, Jiangsu, PR China
[d] Trauma Center, Zhongda Hospital, School of Medicine, Southeast University, Nanjing, Jiangsu, PR China
[e] Department of Geriatrics, Zhongda Hospital, School of Medicine, Southeast University, Nanjing, Jiangsu, PR China

ARTICLE INFO

Keywords:
Tendon stem/progenitor cells
Dipeptide hydrogel
Self-assembly
Growth differentiation factor 5
Tendon repair

ABSTRACT

Owing to the tissue characteristics of tendons with few blood vessels and cells, the regeneration and repair of injured tendons can present a considerable challenge, which considerably affects the motor function of limbs and leads to serious physical and mental pain, along with an economic burden on patients. Herein, we designed and fabricated a dipeptide hydrogel (DPH) using polypeptides P11-4 and P11-8. This hydrogel exhibited self-assembly characteristics and could be administered *in vitro*. To endow the hydrogel with differentiation and regeneration abilities, we added different concentrations of growth differentiation factor 5 (GDF5) to form GDF5@DPH. GDF5@DPH promoted the aggregation and differentiation of tendon stem/progenitor cells and promoted the regeneration and repair of tendon cells and collagen fibers in injured areas. In addition, GDF5@DPH inhibited inflammatory reactions in the injured area. Owing to its injectable properties, DPH can jointly inhibit adhesion and scar hyperplasia between tissues caused by endogenous inflammation and exogenous surgery and can provide a favorable internal environment for the regeneration and repair of the injured area. Overall, the GDF5@DPH system exhibits considerable promise as a novel approach to treating tendon injury.

1. Introduction

Tendons are important tissues that connect muscles and bones and play roles in transmitting strength and maintaining body movement [1,2]. Tendons are prone to injury owing to various conditions, such as excessive exercise, trauma, diabetes, aging, and even rupture, leading to pain and motor dysfunction [3,4]. Moreover, tendon tissues are characterized by poor cellularity and vasculature, which hinder and complicate the healing of tendon injuries [5,6]. Tendon injuries not only lead to the retirement of athletes but also seriously affect the life and labor ability of ordinary people [7–9]. Currently, treatment methods for tendon injuries mainly include conservative treatment and surgical repair [1,10]; however, these methods have limitations. Conservative treatment requires a long recovery period and often fails to fully restore tendon structure and function [11]. Although surgical repair can better address injured tendons, postoperative complications and tendon adhesion also occur [4,12]. Therefore, the effective repair of injured tendons and promotion of tendon regeneration have become important and challenging issues in this field in recent years.

Tendon stem/progenitor cells (TSPCs) are self-renewing pluripotent cells present in tendons and are an important cell source for tendon tissue repair and regeneration [13,14]. TSPCs exhibit can not only differentiate into various cell types, including bone cells, chondrocytes, and adipocytes, but also regulate immune responses and play an

Abbreviations: DPH, dipeptide hydrogel; FTIR, Fourier-transform infrared spectroscopy; GDF5, growth differentiation factor 5; IF, Immunofluorescence; NS, normal saline; ROS, reactive oxygen species; rTSPCs, rabbit tendon stem/progenitor cells; SA, sodium alginate; SAPH, self-assembling peptide hydrogel; SEM, Scanning electron microscopy; SD-PAGE, sulfate-polyacrylamide gel electrophoresis; TEM, transmission electron microscopy; TSPCs, tendon stem/progenitor cells; WB, western blotting.

* Corresponding author. Department of Orthopedics, Zhongda Hospital& School of Medicine, Southeast University, 87 Dingjiaqiao, Nanjing, Jiangsu, 210003, PR China.

E-mail address: ruiyunfeng@126.com (Y.-F. Rui).

https://doi.org/10.1016/j.mtbio.2024.101046
Received 11 January 2024; Received in revised form 31 March 2024; Accepted 2 April 2024
Available online 3 April 2024

important role in maintaining the physiological functions of tendons, including elasticity, flexibility, and tensile strength [15,16]. Rui et al. [17] and Zhang et al. [18] successfully isolated and cultured TSPCs in the tendon tissues of rats and rabbits, respectively, and found that these cells could differentiate toward tendon formation under certain conditions [17]. Therefore, TSPCs play pivotal roles in maintaining tendon homeostasis and promoting tendon injury repair.

Self-assembled polypeptide hydrogels are three-dimensional (3D) network structures comprising polypeptide chains. These polypeptide chains self-assemble into gel-like substances in water. Hydrogels exhibit high water absorption and good biocompatibility and can simulate the extracellular matrix to form a 3D scaffold, which is beneficial for cell growth and tissue regeneration [19–21]. Peptide molecules in self-assembling polypeptide hydrogels usually contain 10–20 amino acids; these peptide molecules can self-assemble into network structures owing to their unique properties [22]. This self-assembly process typically relies on non-covalent bonding interactions, such as hydrophobic interactions, electrostatic interactions, hydrogen bonding, and π–π interactions [23,24]. Compared with traditional biomaterials, self-assembled polypeptide hydrogels exhibit unique characteristics. First, the hydrogel can be used as a drug delivery system to deliver drugs precisely to the repair site in a sustained, metered manner [25–27]. Second, it can support and promote cell proliferation, differentiation, and tissue regeneration, providing favorable conditions for successful tissue engineering [22,28,29]. However, despite the potential applications of self-assembled polypeptide hydrogels for tissue engineering and wound repair, the current therapeutic results are not ideal, especially for tendon repair. Yin et al. [30] found that the RADA peptide hydrogel exhibited good biocompatibility and facilitated TSPCs adhesion and proliferation to a certain extent, preventing the aging of TSPCs; however, the formulated peptide hydrogel failed to substantially promote TSPCs tendon differentiation. Imere et al. [31] found that a self-assembling peptide hydrogel (SAPH) could promote the growth and proliferation of rabbit synovial cells and maintain the production of specific matrix components; however, it did not considerably promote tendon repair in injured tendons. To achieve this, researchers need to incorporate several improvements. First, the physical and chemical properties of self-assembled hydrogels must be improved by optimizing their preparation methods [28,32,33]. Second, other bioactive substances, such as growth factors and cytokines, could be added to promote the proliferation and differentiation of tendon cells [34–36]. These bioactive substances can be embedded into self-assembled hydrogels to provide long-lasting stimulation and promote tendon regeneration.

Growth difference factor 5 (GDF5) is a growth factor belonging to the transforming growth factor category β superfamily. GDF5 plays an important role in the formation and development of bones, joints, and neurons during human growth and development. Furthermore, it has a positive effect on skin healing and recovery [37–39]. Therefore, GDF5 has extensive application prospects in the medical field, especially in the field of regenerative medicine, such as bone and joint repair and nerve injury repair [40,41]. GDF5 also plays a crucial role in the formation and development of tendons. GDF5 promotes the proliferation and differentiation of tendon cells, which is crucial for promoting tendon repair and enhancing tendon function [42–44]. However, effective utilization of this growth factor remains a key issue in scientific research. Moreover, limited research has been conducted on the combined application of GDF5 and polypeptide hydrogels.

In the current study, we used P11-4 and P11-8 polypeptides [45–47] to synthesize an injectable self-assembled dipeptide hydrogel (DPH) under specific conditions and combined it with GDF5 to form a new functional hydrogel, namely GDF5@DPH. Compared with other biomaterials, GDF5@DPH has inherent advantages. Firstly, GDF5@DPH exhibits superior biocompatibility, comprising natural amino acids, which closely resemble the major components of tendons. Additionally, owing to the self-assembly properties of GDF5@DPH, the use of exogenous chemical cross-linking agents can be avoided, leading to improved biocompatibility and biodegradability, thus minimizing immune reactions and foreign body rejection. Secondly, GDF5@DPH has excellent drug-loading capabilities, as it can be precisely controlled by adjusting parameters such as solution temperature and pH, thereby modulating the structure and properties of the hydrogel to achieve sustained drug release and prolonged effects. Thirdly, GDF5@DPH exhibits favorable bioactivity, supporting cell attachment and proliferation, promoting tenogenic differentiation of TSPCs and tendon tissue regeneration, making it suitable for repairing damaged tendon tissue. Lastly, in terms of injectability, GDF5@DPH has suitable viscosity and rheological properties, facilitating injection via a syringe to specific sites for localized treatment or internal tissue injection without the need for surgical implantation. The effects of GDF5@DPH on the proliferation, differentiation, and tendon repair of TSPCs were verified *in vitro* and *in vivo* (Scheme 1). The results of this study will be beneficial for further improving treatment methods for tendon injuries, ultimately enhancing treatment effectiveness and reducing patient pain.

2. Materials and methods

2.1. Preparation of solutions and synthesis of DPH

2.1.1. Preparation of P11-4 and P11-8 polypeptide solutions

The peptide sequence of P11-4 is QQRFEWEFEQQ, with a charge of −2, and the P11-8 peptide sequence is QQRFOWOFEQQ, with a charge of +2, as per the manufacturer's instructions and previous literature [45]. A peptide solution was prepared at a concentration of 2 mg/mL. The peptide powder was exposed to ultraviolet radiation for 60 min. A certain amount of sterile P11-4 and P11-8 powders (Genscript Biotech Corporation, Nanjing, China) was weighed according to the configured concentration and then placed in sterile centrifuge tubes according to the formula ρ = m/V. The corresponding volume of sterile deionized water was added, and the powders were dissolved using vortexing; finally, a peptide solution was obtained at a concentration of 2 mg/mL, which was used for subsequent experiments.

2.1.2. Preparation of the GDF5 solution

In brief, the GDF5 powder (Glpbio, CA, USA) was exposed to ultraviolet radiation for 60 min. Next, 10 μg sterile GDF5 powder was weighed according to the configured concentration and placed in a sterile centrifuge tube according to the formula ρ = Calculate m/V (ρ: density, m: mass, V: volume), followed by the addition of 10 mL of sterile deionized water. The powders were dissolved by oscillation using a vortex instrument to form a solution at a concentration of 5000 ng/mL. Subsequently, the solution was diluted to 5, 25, 50, 100, and 500 (ng/mL) solutions and used for subsequent experiments.

2.1.3. Synthesis of sodium alginate (SA) hydrogel

Following exposure to ultraviolet radiation for 60 min, 4 g of sterile SA powder (Sigma-Aldrich, USA) was weighed and placed into a sterile centrifuge tube, which was calculated according to the formula ρ = m/V. Subsequently, 100 mL sterile deionized water was added, the solution was stirred manually, and placed on a constant-temperature shaking table at 37 °C overnight. The resulting SA hydrogel at a concentration of 4% was used for subsequent experiments.

2.1.4. Synthesis of DPH

The P11-4 and P11-8 solutions were mixed in volume ratios of 100:1, 10:1, 1:1, 1:10, and 1:100. The pH was adjusted to 7.0 using a pH meter (Aquasearcher, OHAUS), and gel formation was observed in a 37 °C incubator.

2.1.5. Synthesis of GDF5-Containing dipeptide hydrogel (GDF5@DPH)

P11-4 and P11-8 solutions were prepared as a mixed solution at a specific volume according to a volume ratio of 10:1. Five parts of the mixed solution comprising 10:1 P11:P12 were selected, and GDF5

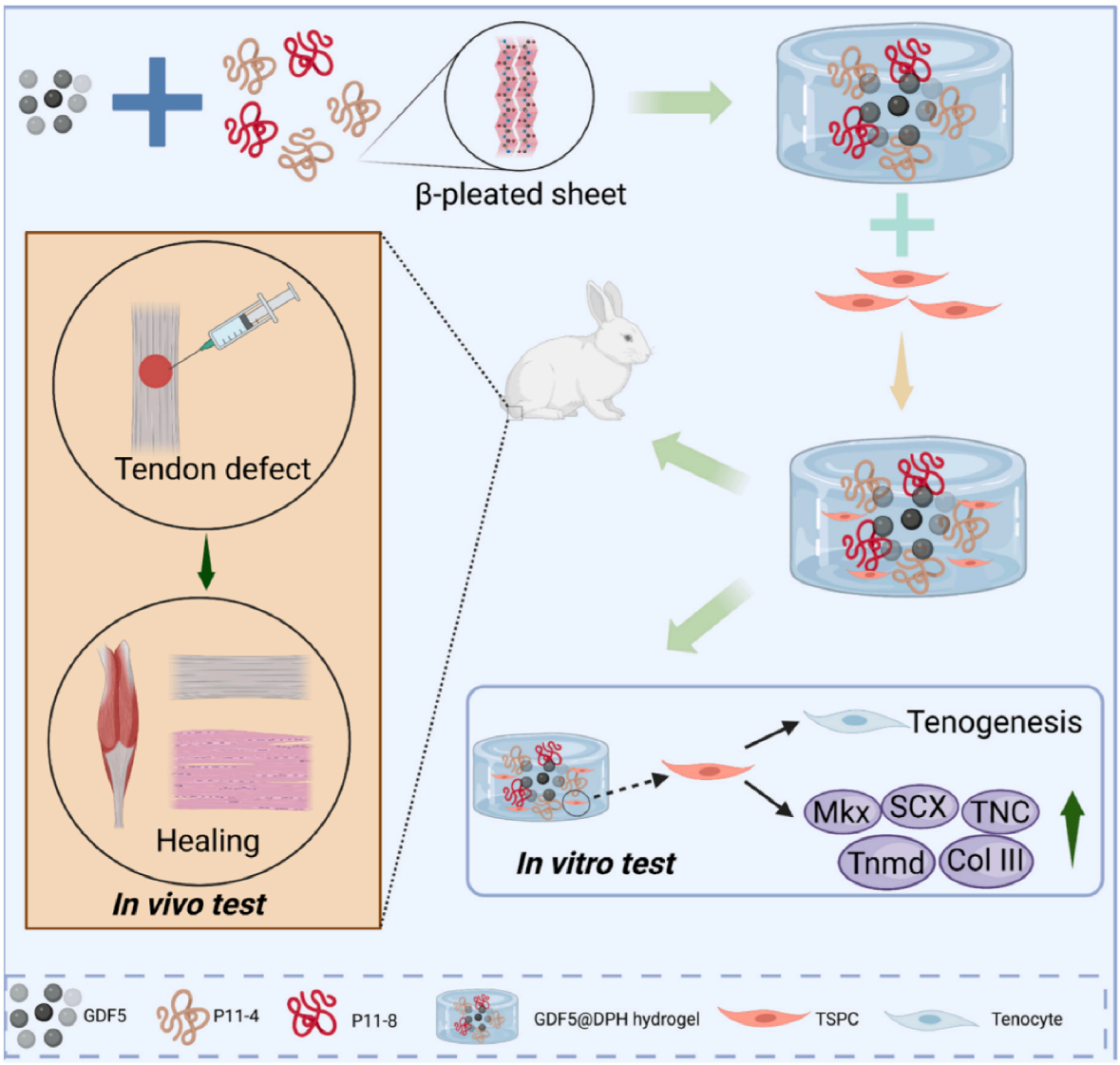

Scheme. 1. Principle underlying GDF5@DPH synthesis and its mechanism for promoting tendonogenic differentiation of TSPCs and tendon repair. TSPCs, tendon stem/progenitor cells; GDF5, growth difference factor 5; DPH, dipeptide hydrogel.

solutions at different volumes and concentrations of 5000 ng/mL were added, respectively. The pH value of the mixed solution was adjusted to 7.0, and the mixed solution was placed in a 37 °C incubator for gelation. Finally, functional DPHs containing GDF5 concentrations of 5, 25, 50, 100, and 500 ng/mL were achieved (5-GDF5@DPH, 25-GDF5@DPH, 50-GDF5@DPH, 100-GDF5@DPH, and 500-GDF5@DPH, respectively).

2.2. Characterization and physicochemical properties of hydrogels

2.2.1. Tilt test

In the centrifuge tubes, 1 mL of mixed solutions with different ratios or concentrations were prepared. The centrifuge tubes were placed in a 25 or 37 °C constant temperature chamber, and each group of centrifuge tubes were tilted every 1–5 min to observe the fluid state of the mixed solutions.

2.2.2. Scanning electron microscopy (SEM)

After freeze-drying hydrogels for 24 h, test samples were collected and then sputter-coated with gold. The microstructures of the materials were observed using SEM (SEM Zeiss Supra 55, Germany).

2.2.3. Measurement and calculation of pore size and porosity

SEM images were used to analyze the pore sizes of the freeze-dried hydrogels using ImageJ 1.51j8 (National Institutes of Health, Bethesda, MD). The porosity was calculated using the ethanol exchange method [48]. The dried hydrogels were weighed (Wh) and immersed in absolute ethanol to obtain the wet weight (Wa). The porosity of the hydrogel was calculated according to the following equation: Porosity = Wa-Wh/ρV, where ρ represents the density of ethanol and V represents the volume of dried hydrogel.

2.2.4. Fourier-transform infrared spectroscopy (FTIR)

SA, DPH, and GDF5@DPH (2 mL, n = 3) were freeze-dried for 24 h, and the samples were collected. FTIR spectra of the three hydrogels were measured using an FTIR spectrophotometer (Thermo Scientific Nicolet iS20, USA). Spectra were obtained after 32 scans in the range of 4000–400 cm^{-1} with a resolution of 4 cm^{-1}.

2.2.5. Water contact angle

The contact angle of each hydrogel material on hydrophilic polyethylene was measured using an optical surface analyzer (OSA 100, L10018A302, Lauda Scientific, Germany). The hydrogel liquid was dropped onto the hydrophilic polyethylene, and the contact angle was

recorded when the liquid was stabilized on the surface.

2.2.6. In vitro degradation of the hydrogels

In brief, 2 mL of hydrogel (n = 4) was lyophilized for 24 h to obtain a xerogel (D0), which was then completely immersed in 1 mL of simulated body fluid placed in a shaker at 37 °C and 100 rpm. At each test point, the hydrogel was removed and placed it in dH_2O overnight in an oven at 37 °C to determine the weight of the xerogel (D1). Weight remaining (%) = D1/D0 [49].

2.2.7. Equilibrium water content

Seven groups of hydrogels (2 mL, n = 4) were immersed in phosphate-buffered saline (PBS) for 24 h and freeze-dried for 24 h to obtain dry gels. The equilibrium moisture content was calculated by reducing the weight before and after freeze-drying using the following formula: Equilibrium water content = Cw-Cd/Cw, where Cw and Cd refer to the weights of wet and dry hydrogels, respectively [50].

2.2.8. Evaluation of sustained-release concentration of GDF5

Hydrogels containing different concentrations of GDF5 (1 mL, n = 4) were immersed in the same amount of simulated body fluid, and the extracts from each group were collected after 1, 4, 7, 10, 14, 21, 28, and 35 days. An ELISA kit (Zeye Bio-Technology Co., Ltd., Shanghai, China) was used for quantitative detection of GDF5.

2.2.9. Evaluation of the rheological properties

The rheological properties were evaluated using a rheometer (Anton Paar, Graz, Austria). Dynamic frequency sweep was performed at 1% strain from 0.1 to 100 rad/s, dynamic strain sweep was performed at 0.1%–100% strain at a rate of 10 rad/s, dynamic shear rate sweep was performed in the range of 0.1–10 s^{-1}, and viscosity was measured [50].

2.3. In vitro experiments

2.3.1. Isolation and culture of rabbit TSPCs (rTSPCs)

rTSPCs were isolated and cultured as described previously [18]. TSPCs were obtained from six female New Zealand white rabbits (8–10 weeks old, 3.0–4.0 kg). After the rabbits were euthanized, the middle sections of Achilles tendon tissue or patellar tendon tissue were dissected, and the connective tissue surrounding the tendon was carefully excised. After cutting, the specimens were digested with collagenase type I (3 mg/mL; Sigma-Aldrich, St. Louis, MO, USA) for 1.5 h. Single-cell suspensions were established by filtering through a 70 μm filter, and cells were incubated in DMEM (Thermo Fisher Scientific, USA) containing 10% (v/v) fetal calf serum (Thermo Fisher Scientific, USA) and 1% (v/v) penicillin-streptomycin (Thermo Fisher Scientific, USA) at 37 °C under 5% CO_2 for 7–10 days. After clone formation was observed under a microscope, primary cells (P0) were mixed and labeled by trypsin digestion. P3–P5 cells were used for the subsequent experiments. The culture medium was changed every three days during the experiment.

2.3.2. Cell seeding onto hydrogel of each group

Each group of hydrogels was injected into 96-well plates at 100 mL per well and placed in an incubator at 37 °C and 5% CO_2 for 1 h to adapt to the physiological environment. rTSPCs were then seeded on each hydrogel in 96-well plates at 37 °C under 5% CO_2. The culture medium was changed every day.

2.3.3. Cell viability

The cell viability was examined using a live/dead kit (Invitrogen, UK). In brief, rTSPCs were seeded in 96-well plates at a density of 10^4 cells/well. After incubating cells for 3 and 7 days in each hydrogel group, 2 mL of PBS containing 2×10^{-6} M calcein AM and 4×10^{-6} M EthD-1 solution were added. Then, 200 μL of live/dead solution was added, and the sample was incubated for 30 min at room temperature. Samples were washed twice with PBS. Images were captured using an inverted fluorescence microscope (Leica DM IL LED Fluo; Leica Microsystems, Germany) with excitation filters at 494 nm (green, calcein AM) and 528 nm (red, EthD-1). The nuclei of living and dead cells were stained green and red, respectively.

2.3.4. Cell proliferation

The proliferation of rTSPCs was analyzed using Cell Counting Kit-8 (CCK-8; Sigma Aldrich). rTSPCs were cultured in 96-well plates at a primary density of 5×10^3 cells/well for 1, 3, 5, and 7 days. The cells were incubated with 10% CCK-8 for 1.5 h. The absorbance was measured at 450 nm using a microplate reader (Synergy 2; BioTek, USA).

2.3.5. Reverse transcription-quantitative polymerase chain reaction (RT-qPCR)

After 7 days of TSPC cultivation, total RNA was extracted from the TSPC-loaded hydrogel using TRIzol reagent (Invitrogen, Carlsbad, Calif., USA). Complementary genes were synthesized by reverse transcription of 2 μg template RNA in a two-step RT-qPCR SuperMix kit (TransGen Biotech, China) according to the manufacturer's instructions [51]. RT-qPCR was performed using an ABI 7500 system (Thermo Fisher Scientific, USA). Relative gene expression levels were normalized to the housekeeping gene GAPDH to obtain relative gene expression fold values and calculated using the $2^{-\Delta\Delta}$ cycle threshold ($2^{-\Delta\Delta Ct}$) method. For the primer (Nanjing Bolaz Biotechnology Co., Ltd. China) sequences used, please see Supplementary Table S1.

2.3.6. Western blotting (WB) assay

WB was performed after incubating TSPCs with a water gel for 7 days to evaluate protein expression levels. Cellular proteins were extracted using a Total Protein Extraction Kit (Beyotime Biotechnology, Shanghai, China). A BCA protein analysis kit (Beyotime Biotechnology, Shanghai, China) was used to completely mix the proteins in the supernatant with sodium dodecyl sulfate-polyacrylamide gel electrophoresis (SDS-PAGE) protein loading buffer (5 ×) (Beyotime Biotechnology) at a volume ratio of 4:1. The obtained proteins were heated at 100 °C for 10 min for denaturation. Using 4–20% SDS-PAGE (ACE Biotechnology, Beijing, China), the same amount of protein (30-mg system) was transferred onto a polyvinylidene fluoride (PVDF) membranes (Sigma, USA). The membranes were blocked in a blocking solution (Beyotime; China) for 1 h, washed in TBST (Servicebio; China), and incubated with an untagged F(ab')2 Fragment Goat Anti-Rabbit IgG (H + L) (30 μg/mL; 111-006-003, Jackson ImmunoResearch) at 36 °C for 2 h. After washing again, membranes were incubated with primary antibodies overnight at 4 °C. After washing, membranes were incubated with secondary HRP-conjugated antibodies for 1 h at room temperature. Imaged, and visualized using a ChemiDoc MP imaging system (Bio-Rad, CA, USA). Protein band intensity was quantified using ImageJ (NIH) and standardized to the corresponding GAPDH band (National Institutes of Health MD, Bethesda, USA). The antibody information is listed in Supplementary Table S2.

2.3.7. Immunofluorescence (IF) assay

The cell culture medium was removed from each group, and the cells were washed three times with PBS. Cells were fixed with cold paraformaldehyde (4%; Biosharp, Hefei, China) for 20 min, washed thrice with PBS for 5 min each, and then shaken. Samples were disrupted using Triton X-100 (0.25%; Sigma-Aldrich) for 15 min, washed three times in PBS for 5 min each, and shaken. Then, the samples were incubated with immunostaining blocking solution (Beyotime Biotechnology) for 60 min, followed by the addition of the primary antibody (primary antibody dilution mixture). The sample was maintained under shaking overnight at 4 °C. The primary antibody was removed, and samples were washed three times with PBS for 5 min each time and shaken. Next, the samples were incubated with secondary antibodies and Alexa Fluor 488

and 647 (Beyotime Biotechnology, China) at room temperature for 60 min in the dark. The secondary antibody was recovered, and samples were washed three times with PBS and shaken for 5 min. Subsequently, 100 μL 4′, 6-diamidino-2-phenylindole (DAPI; Sigma-Aldrich, USA) was added, and samples were incubated for 15 min in the dark. The samples (membranes) were washed three times with PBS for 5 min each. Detection was performed using an inverted fluorescence microscope (Leica DM IL LED Fluo; Leica Microsystems, Germany). The antibody information is listed in Supplementary Table S2.

2.4. In vivo experiments

2.4.1. Animal model

All surgical interventions and postoperative animal care were performed in accordance with the National Research Council's Guide for the Care and Use of Laboratory Animals and approved by the Animal Research Ethics Committee of Southeast University (No. 20220816006). Thirty New Zealand white rabbits (2.5–3 kg, 6 months) were randomly divided into five groups of six rabbits each. After administering a pentobarbital sodium injection, a hole (diameter: 4 mm, height: 1.5 mm) was punched to induce an Achilles tendon tissue defect in the bilateral medial Achilles tendon, and normal saline (NS), SA, DPH, GDF5@DPH, and GDF5@DPH + TSPCs were injected into the defects. The incisions were then sutured. The rabbits were housed in a humidity-controlled room at 25 °C, under a 12-h light/dark cycle, with free access to food and water.

2.4.2. Transmission electron microscopy (TEM)

Tissue specimens were fixed using standard TEM procedures to assess the collagen fibril diameter and alignment. Operational steps were performed as detailed previously [52].

2.4.3. Mechanical testing

After six weeks of feeding, the rabbits were sacrificed, and the bilateral Achilles tendons were harvested for mechanical testing. Mechanical testing was performed using the Instron tension/compression system with FastTrack software (Model 5543, Instron, Canton, MA, USA). The structural properties of Achilles tendons are represented by their modulus (MPa), failure force (N), and stress at failure (MPa). Operational steps were performed as detailed previously [53].

2.4.4. Histopathological evaluation

Six weeks postoperatively, the regenerated tendons were harvested, fixed in 4% buffered formalin for 24 h, dehydrated in an ethanol series, and embedded in paraffin. Longitudinal sections of tendons were cut into 7-μm thick slices. The slides were dewaxed, rehydrated, and stained with hematoxylin and eosin (H&E), Masson's trichrome, and Sirius red.

2.4.5. Enzyme-linked immunosorbent assay (ELISA)

Two weeks postoperatively, rabbits were anesthetized, and Achilles tendon tissues were harvested. The Achilles tendon tissues were cut, mechanically homogenized in 0.9% NS at 200 mg/mL, and centrifuged at 12,000 rpm for 10 min at 4 °C. The supernatant was collected to perform ELISA and the concentrations of interleukin (IL)-1β, IL-6, and tumor necrosis factor (TNF)-α were determined using Rabbit IL-1 β ELISA Kit (Sigma-Aldrich, USA), Rabbit IL-6 ELISA Kit (Reanta, Beijing, China), and Rabbit TNF-a ELISA Kit (Shanghai Enzyme-linked Biotechnology Co., Ltd., China), respectively, in accordance with the manufacturer's instructions.

2.5. Statistical analysis

All data are presented as the mean ± standard deviation (SD). Data analyses were analyzed using SPSS version 26.0 (IBM Corp., Armonk, NY, USA). GraphPad Prism 8.4 (GraphPad Software, CA, USA) was used to prepare the graphical representation. After analyzing the normality using the Shapiro-Wilk test, two-group comparisons were performed using the independent *t*-test and nonparametric test. Multiple groups were compared using one-way analysis of variance (ANOVA) and post hoc tests. $P < 0.05$ was considered statistically significant.

3. Results

3.1. Synthesis and characterization of in-situ injectable DPH

The molecular structures of the P11-4 and P11-8 polypeptide sequences were determined. The two polypeptides were cross-linked with each other through electrostatic interactions, hydrophobic interactions, and π–π stacking bonds (Fig. 1A). At a P11-4 to P11-8 vol ratio of 10:1 and pH was 7.0, the mixed solution formed a gel at 37 °C with a gelation time of 417 ± 11 s, which was convenient for clinical injection operation (Fig. 1B). At 25 °C, the gelation time of the mixed solution was prolonged, which was not conducive to clinical operation (Fig. 1C). When different concentrations of GDF5 were added to the mixed solution of dipeptides, the gelation time showed no significant change (Fig. 1D). During the experiment, DPH and GDF5@DPH had injectable characteristics and could be injected into various shapes (Fig. 1E).

3.2. Characterization of the DPH and GDF5@DPH

The freeze-dried hydrogels of each group were analyzed by SEM, and the results revealed that all hydrogels exhibited a porous structure. The SA group exhibited smaller pores, whereas the DPH and GDF5@DPH groups exhibited larger pores. According to energy dispersive spectroscopy, the DPH and GDF5@DPH groups were mainly composed of carbon (C), nitrogen (N), and oxygen (O) (Fig. 2A). Based on quantitative analysis, the DPH and GDF5@DPH groups had larger pore sizes and higher porosities than the SA group, with the 100-GDF5@DPH group exhibiting the most notable advantages (Fig. 2B–C). FTIR revealed a strong absorption peak at 3431 cm^{-1} for the DPH and GDF5@DPH groups, indicating the presence of amino groups (-NH2). The strong absorption peak at 2950 cm^{-1} suggests the presence of methylene groups ($–CH_2$). The appearance of strong absorption peaks in the range of 1632–1637 cm^{-1} indicated the possible existence of β-folded secondary structures (Fig. 2D). In addition, dynamic frequency sweep rheological tests were performed to examine the viscoelasticity and stability of the hydrogels at different temperatures. The storage modulus (G′) and loss modulus (G″) were recorded as a function of the frequency and time, with a higher G′ than G″ indicating fast gelation. At 25 °C, within the range of 0.1–100 rad/s, the SA group had the highest G′ value, indicating a higher elastic modulus. The DPH group showed an increasing trend in G′ after the addition of GDF5, indicating a more compact crosslinked network. Furthermore, the G′ values of all groups gradually decreased, indicating a decrease in the elastic modulus and a shift toward a more viscous liquid phase (Fig. 2E). Compared with that at 25 °C, the G′ value of the hydrogels in all groups increased at 37 °C, indicating a higher elastic modulus and stronger structure at 37 °C, which is favorable for gelation (Fig. 2F).

According to the water contact angle test results, the SA group had a contact angle of 59.67 ± 1.53°, whereas the DPH and GDF5@DPH groups had significantly reduced contact angles, indicating higher hydrophilicity in the DPH and GDF5@DPH groups (Fig. 3A–H). Similarly, the water content experiment revealed that the DPH and GDF5@DPH groups had higher water contents than the SA group, suggesting better hydrophilicity (Fig. 3I). The degradation test showed that the SA group degraded slowly within 35 days, whereas the DPH and GDF5@DPH groups degraded gradually, indicating better degradation properties and reduced residues in the body (Fig. 3J). According to the results of the drug release experiment, the hydrogel containing a high GDF5 peptide concentration released a higher concentration at each time point. After approximately 28 days, GDF5 was almost completely released from the hydrogel, indicating the good release efficiency of GDF5@DPH

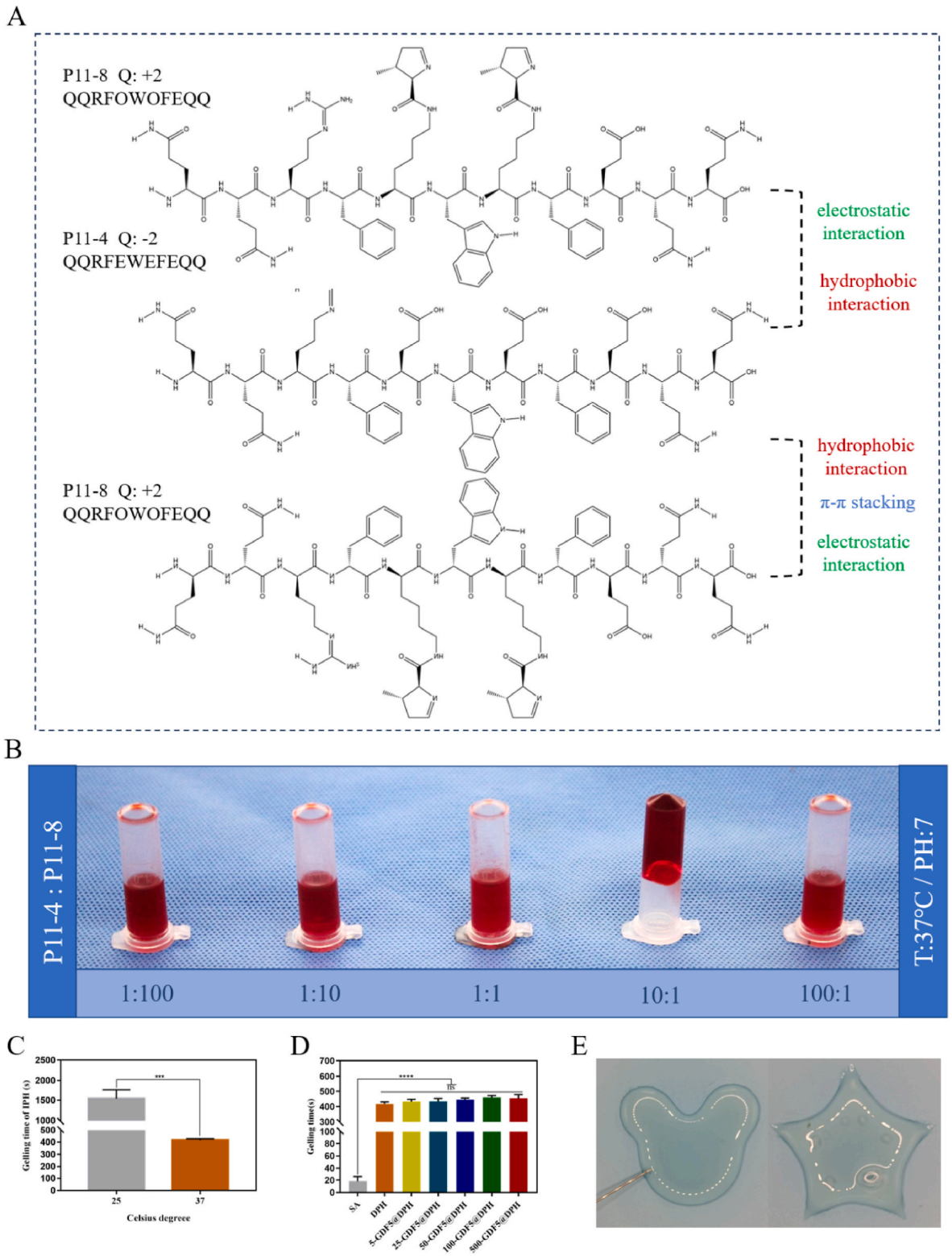

Fig. 1. Structural composition and gel-forming characteristics of DPH. (A) Molecular structure and binding mode of polypeptides P11-4 and P11-8. (B) Gelling conditions of DPH (red dye was added to observe gel formation). (C) Gelation time of DPH at different temperatures. (D) Gelation time of DPH combined with different concentrations of GDF5. (E) Injectable properties of DPH. Data are presented as the mean ± standard deviation. n = 4 for each group, ns: not significant, ***P < 0.001, ****P < 0.0001. DPH, dipeptide hydrogel; GDF5, growth difference factor 5; SA, sodium alginate. (For interpretation of the references to colour in this figure legend, the reader is referred to the Web version of this article.)

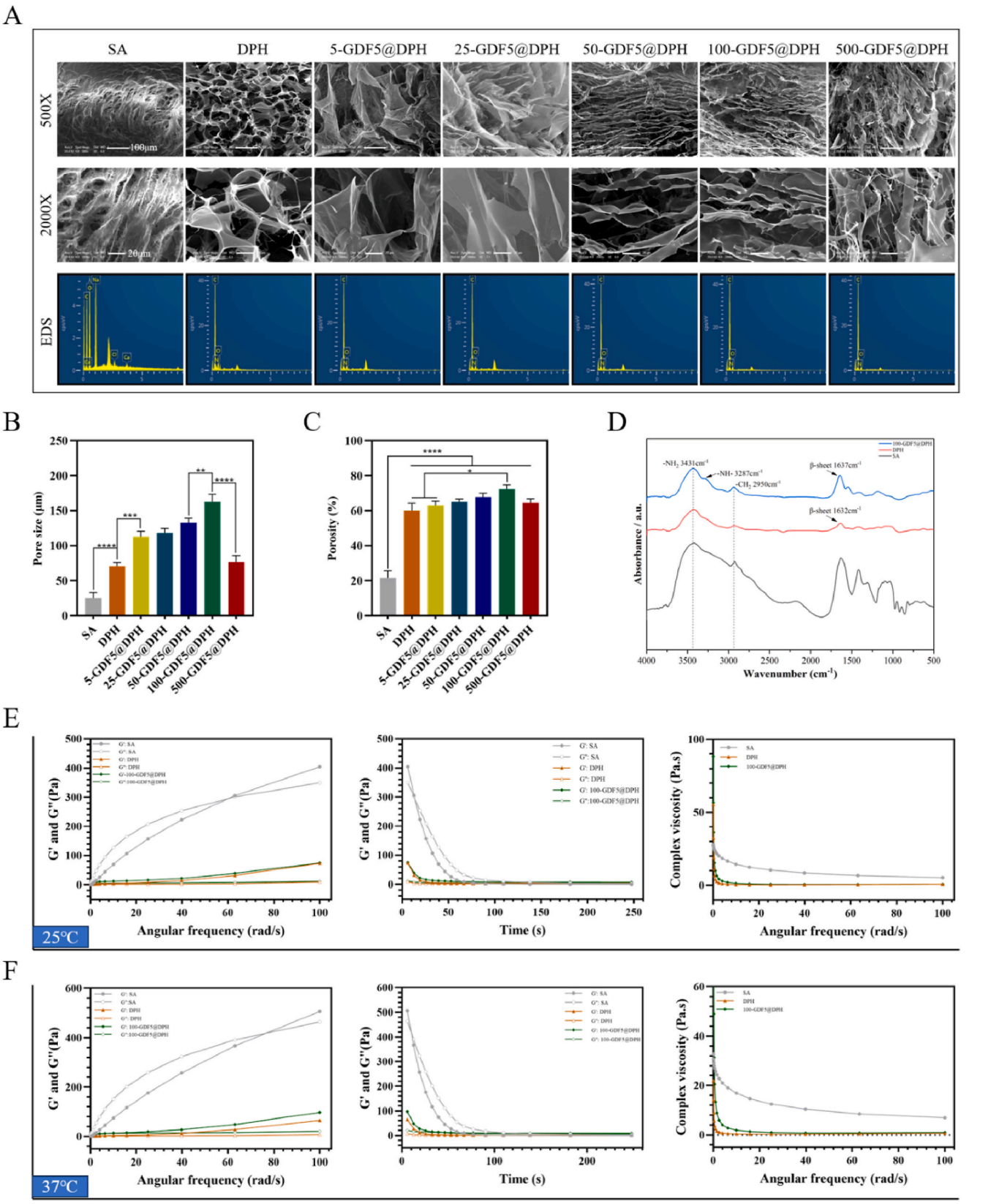

Fig. 2. Characterization and fluid properties of the hydrogels. (A) SEM and energy spectrum analysis. (B–C) Quantitative analysis of the pore size and porosity. (D) FTIR analysis of functional groups and secondary structures. (E–F) The rheological properties of the hydrogels were analyzed at different temperatures. Data are presented as the mean ± standard deviation. n = 3 for each group, *P < 0.05, **P < 0.01, ***P < 0.001, ****P < 0.0001. SEM, scanning electron microscope; FTIR, Fourier-transform infrared spectroscopy; DPH, dipeptide hydrogel; SA, sodium alginate.

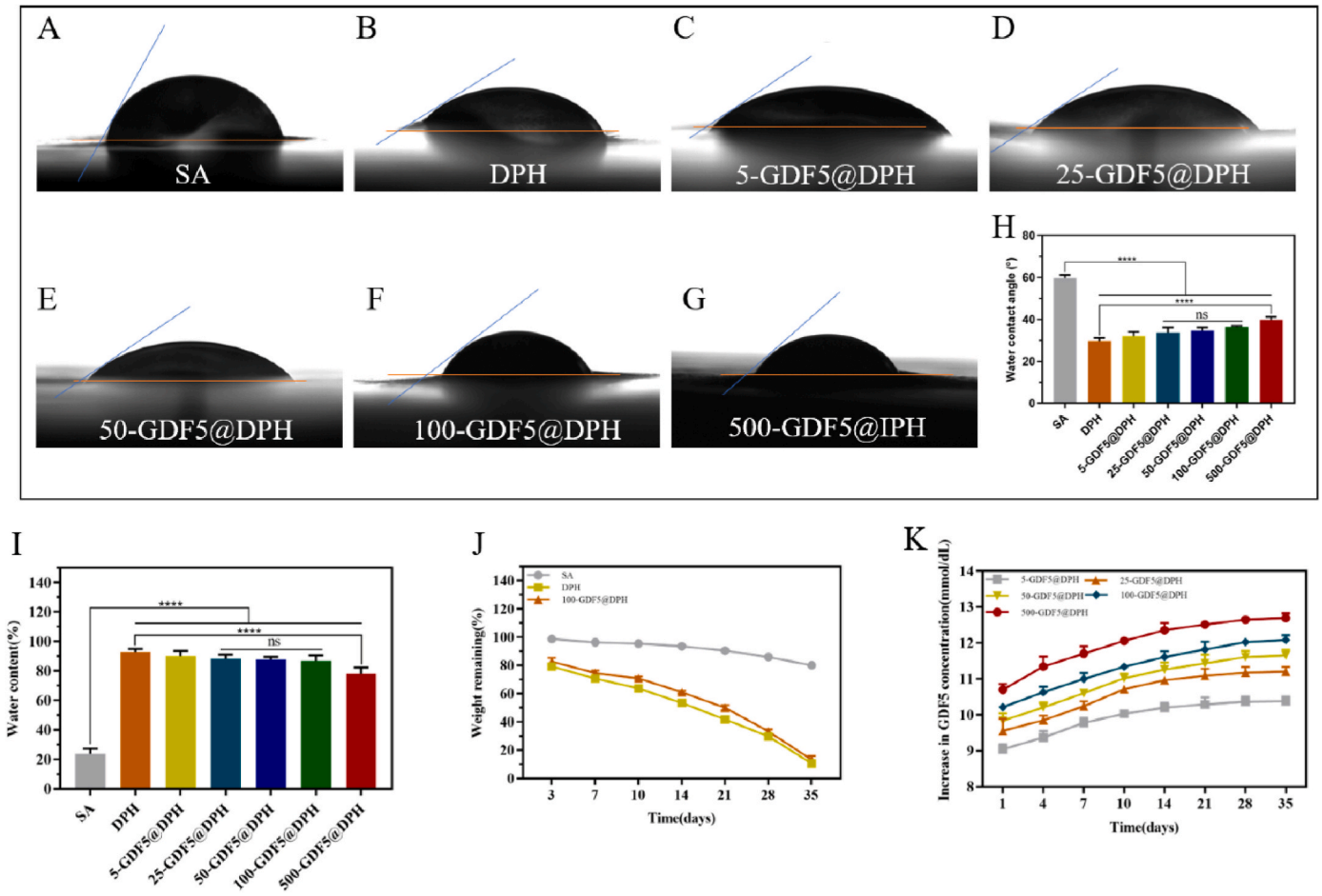

Fig. 3. Hydrophilicity, degradation, and sustained-release characteristics of hydrogels. (A) Water contact angle and quantitative analysis. (B) Water content analysis. (C) Hydrogel degradation characteristics of each group. (D) GDF5 sustained-release test. Data are presented as the mean ± standard deviation. n = 4 for each group, ns: not significant, ****P < 0.0001. DPH, dipeptide hydrogel; SA, sodium alginate; GDF5, growth difference factor 5.

(Fig. 3K).

3.3. Cytotoxicity and biocompatibility of DPH and GDF5@DPH in vitro

TSPCs were seeded into the wells of each group and co-cultured. After 3 and 7 days, TPSCs were observed under a light microscope, revealing that TSPCs in the hydrogel group grew in aggregates when compared with the flat growth observed in simple wells. The degree of aggregate growth in the DPH and GDF5@DPH groups was significantly higher than that in the SA group, with the 50- and 100-GDF5@DPH groups exhibiting the most significant levels of cell aggregation (Fig. 4A). Additionally, cells were stained using live/dead staining and analyzed using laser confocal scanning after 3 and 7 days. Herein, TSPCs grew as 3D aggregates in the hydrogel instead of the flat growth observed in simple wells. The double-peptide hydrogel group exhibited significantly more live cells and fewer dead cells than the SA group. The 50- and 100-GDF5@DPH groups exhibited stronger live cell growth and aggregation (Fig. 4B). Quantitative analysis also revealed that TSPCs in the hydrogel had stronger activity than those in the 2D and SA groups, with the 100-GDF5@DPH group displaying the best performance (Fig. 4C–D). A CCK-8 assay was performed to measure the optical density (OD) values of cells from each group at 1, 3, 5, and 7 days post-culture. On day 1, the 2D culture group had higher OD values than the 3D culture group. However, on days 3, 5, and 7, the OD values of the DPH and GDF5@DPH groups were significantly higher than those of the 2D group. The 25-, 50-, and 100-GDF5@DPH groups exhibited high OD values. The OD values of the SA group remained consistently lower than those of the 2D group (Fig. 4E). According to the cell cycle results, the percentage of TSPCs in the S phase of the cell cycle was increased in the DPH and GDF5@DPH groups when compared with that in the SA group (Fig. S1). Additionally, we co-cultured TSPCs with the hydrogels of each group for 7 days and examined pores using SEM. The DPH and GDF5@DPH groups had larger pores than the SA group, which was more favorable for the growth and spread of TSPCs (Fig. 4F). Furthermore, TSPCs were co-cultured with the hydrogels of each group for 3 days and cytoskeleton staining revealed that the DPH and 100-GDF5@DPH groups had a more expanded cytoskeleton morphology than the SA group; this was beneficial for cell proliferation and migration (Fig. S2). The scratch test revealed that TSPCs in the DPH and GDF5@DPH groups had stronger migration abilities than those in the SA group (Fig. S3).

3.4. GDF5@DPH promotes tendonogenic differentiation of rTSPCs

To perform IF analysis, TSPCs were seeded into the wells of each group, followed by co-culturing for 7 days. Laser confocal scanning was performed to detect the expression of the tendon-related proteins scleraxis (SCX) and collagen III (COL-III) in the TSPCs of each group. The immunofluorescence intensities of SCX and COL-III in TSPCs of the GDF5@DPH group were significantly higher than those of the SA and DPH groups, with the 100-GDF5@DPH group exhibiting the strongest fluorescence intensity (Fig. 5A–C). Additionally, RT-qPCR experiments revealed that the expression of the tendon-related genes *SCX*, *TNC*, *MKX*, and *Tnmd* was higher in the GDF5@DPH group than in the SA and DPH groups, with the 100-GDF5@DPH group showing the most significant

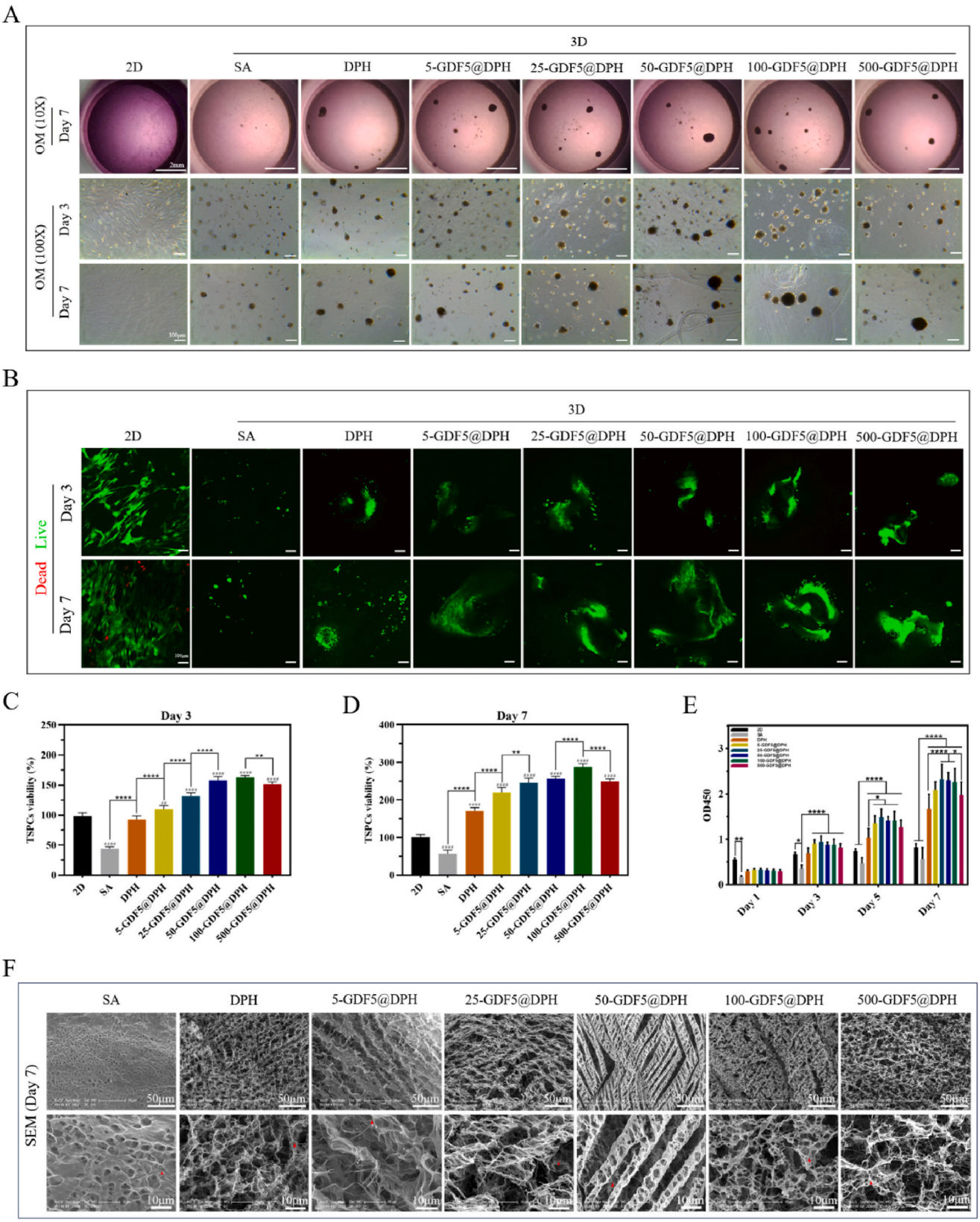

Fig. 4. Cytotoxicity and biocompatibility testing. (A) TSPCs were examined by optical microscopy after co-culturing with each group of hydrogels for 3 and 7 days. (B) Changes in the number of living and dead cells after co-culturing TSPCs in hydrogel for 3 and 7 days by live-dead staining. (C–D) The viability of TSPCs after 3 and 7 days of cu-culture. (E) Quantitative analysis of absorbance values at different time points in each group. (F) The quantity and morphology of TSPCs in hydrogels examined by SEM after 7 days of co-culture (Red triangle represents cells). Data are presented as the mean ± standard deviation. n = 4 for each group, # indicates comparison with the 2D group, $^{\#\#}P < 0.01$, $^{\#\#\#\#}P < 0.0001$, $^{**}P < 0.01$, $^{****}P < 0.0001$. Scale bars: 2 mm and 100 μm. TSPCs, tendon stem/progenitor cells; DPH, dipeptide hydrogel; SA, sodium alginate; SEM, scanning electron microscopy; 2D, two-dimensional; 3D, three-dimensional. (For interpretation of the references to colour in this figure legend, the reader is referred to the Web version of this article.)

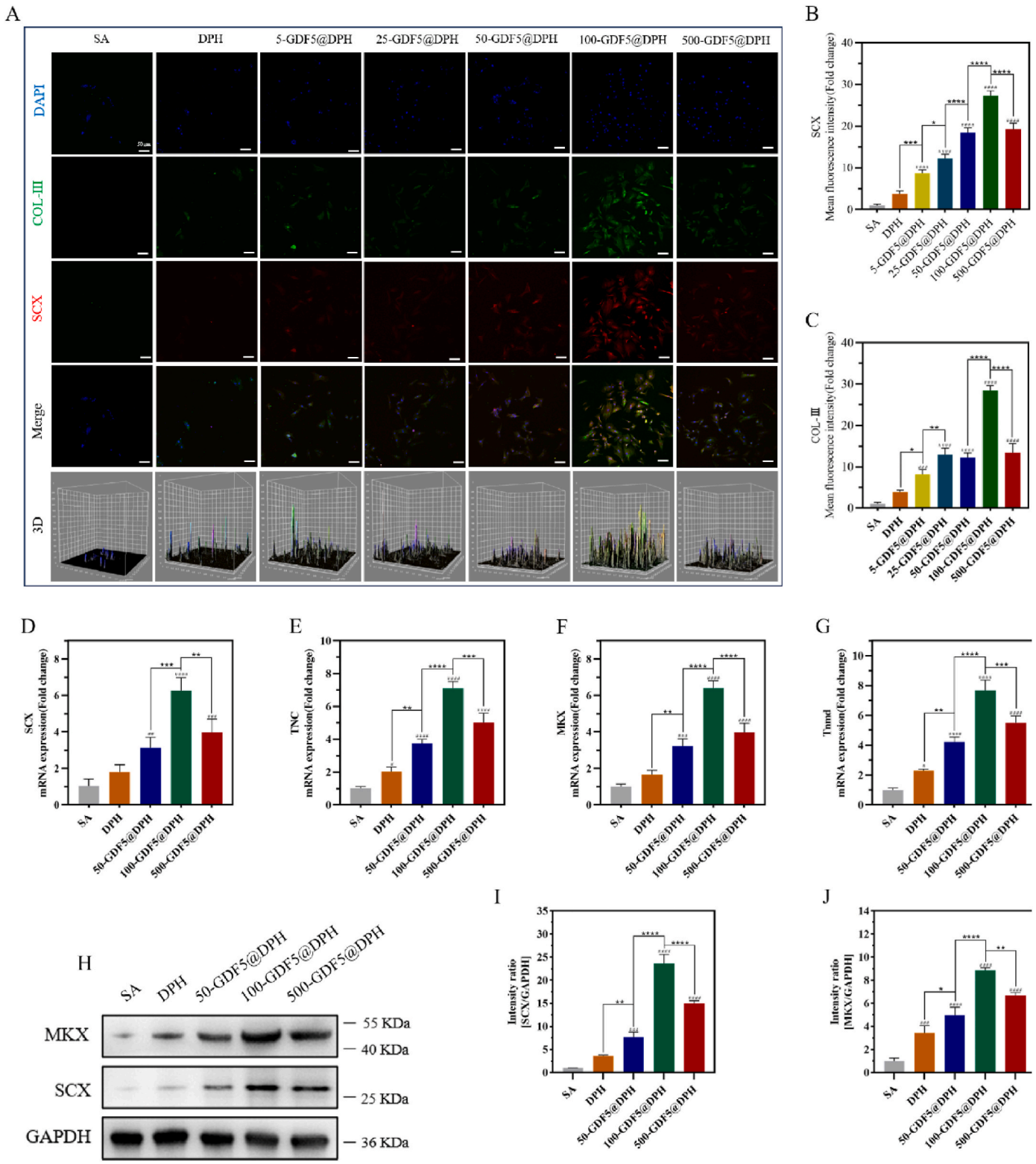

Fig. 5. GDF5@DPH promotes tendonogenic differentiation of TSPCs. (A–C) IF was used to observe the fluorescence intensity and correlation semi-quantitative analysis of tendon-related proteins SCX and COL-III in the TSPCs of each group. (D–G) RT-qPCR was used to detect the gene expression differences of tendonogenesis-related genes *Scx*, *Tnc*, *Mkx*, and *Tnmd* in TSPCs. (H–J) WB analysis was performed to determine the expression of tendinosis-related proteins SCX and MKX in TSPCs and for semi-quantitative analysis. All full-length blots are presented in Additional File 2: Fig. 5H. Data are presented as the mean ± standard deviation. n = 3 for each group, # stands for comparison with SA group, $^{\#}P < 0.05$, $^{\#\#}P < 0.01$, $^{\#\#\#}P < 0.001$, $^{\#\#\#\#}P < 0.0001$, $^{*}P < 0.05$, $^{**}P < 0.01$, $^{***}P < 0.001$, $^{****}P < 0.0001$. Scale bar: 50 μm. IF, immunofluorescence; TSPCs, tendon stem/progenitor cells; DPH, dipeptide hydrogel; SA, sodium alginate; SEM, scanning electron microscopy; 3D, three-dimensional; RT-qPCR, reverse transcription-quantitative polymerase chain reaction; WB, western blotting; SCX, Scleraxis; TNC, Tenascins; MKX, Mohawk; Tnmd, Tenomodulin; COL-III, Collagen III.

increase (Fig. 5D–G). Similarly, WB analysis indicated that the expression of tendon-related proteins SCX and MKX was higher in the GDF5@DPH group than in the SA and DPH groups, with the 100-GDF5@DPH group displaying the most prominent protein bands (Fig. 5H–J). Furthermore, TSPCs were co-cultured with hydrogels for 7 days and then detected by RT-qPCR. The expression of *COL-I*, *PCNA*, and *α-SMA* in DPH and 100-GDF5@DPH groups was higher than that in the SA group, with the GDF5@DPH group exhibiting the most notable effect (Fig. S4). Compared with the SA and DPH groups, the 100-GDF5@DPH group exhibited increased membrane potential (Fig. S5) and decreased intracellular ROS levels (Fig. S6) in TSPCs. These findings suggested that 100-GDF5@DPH may inhibit oxidative stress responses within TSPCs. Overall, the experimental results suggest that the 100-GDF5@DPH group exhibited a superior ability to promote tendon differentiation of TSPCs. Therefore, this hydrogel group was used to perform subsequent *in vivo* experiments to validate their ability to promote tendon repair and regeneration.

3.5. GDF5@DPH and GDF5@DPH loaded with exogenous TSPCs enhance tendon regeneration and repair in vivo

The main steps of constructing a rabbit Achilles tendon injury model and intervention are shown in Fig. 6A–D. The various groups of hydrogels were separately injected into the Achilles tendon defect. The GDF5@DPH + TSPCs group consisted of a mixture of autologous patellar tendon-derived TSPCs (P3) and GDF5@DPH (1×10^6 cells/mL). Three weeks after implantation, heart, liver, spleen, lung, kidney, and brain specimens from each group were subjected to histological

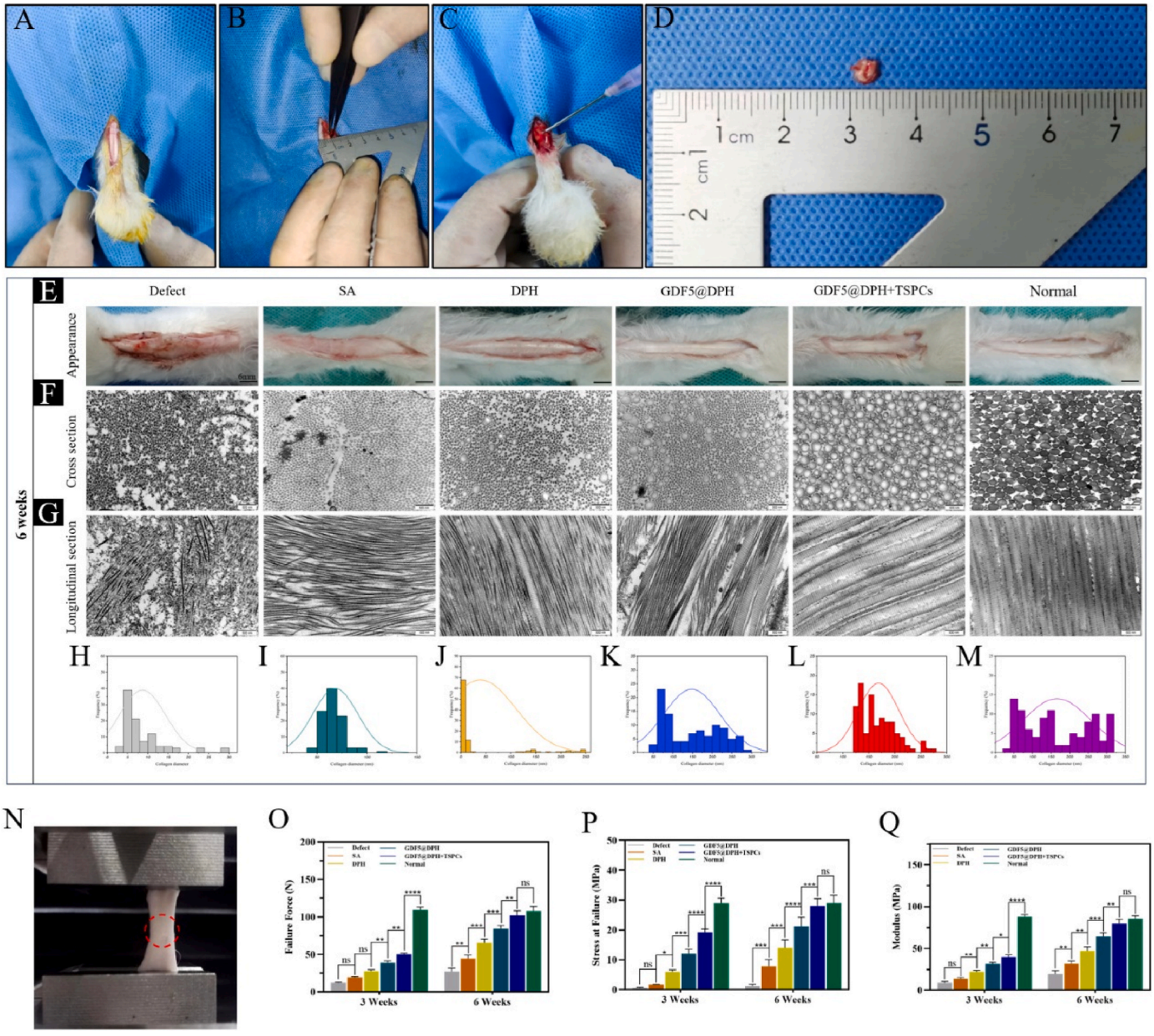

Fig. 6. GDF5@DPH and GDF5@DPH loaded with exogenous TSPCs promote regeneration and the mechanical properties of injured Achilles tendon. (A–D) Rabbit Achilles tendon defect model and main operating procedures. (E) Apparent morphology of the Achilles tendon of rabbits in each group at 6 weeks post-surgery. (F–G) TEM was used to examine the fiber structure of the Achilles tendon in each group. (H–M) Distribution of the diameter frequency of collagen fibrils in the Achilles tendon of each group. (O–R) Analysis of the mechanical properties of the Achilles tendon in each group. Data are presented as the mean ± standard deviation. n = 3 for each group, ns: not significant, *P < 0.05, **P < 0.01, ***P < 0.001. Scale bar: 6 mm. TSPCs, tendon stem/progenitor cells; DPH, dipeptide hydrogel; SA, Sodium alginate; NS, normal saline; GDF5, growth difference factor 5.

assessment (Fig. S7). Simultaneously, the blood of rabbits in each group was also examined to determine changes in indicators of liver and kidney function, myocardial enzymes, and other indicators (Fig. S8). Compared with healthy rabbits, rats injected with DPH and GDF5@DPH into the Achilles tendon defect did not exhibit any notable damage to major organs and disturbances in blood parameters. Moreover, six weeks after surgery, the rabbits in the defect and SA groups showed soft and swollen Achilles tendon tissue, whereas those in the DPH group generally improved, while the GDF5@DPH and GDF5@DPH + TSPCs groups had no apparent swelling, with harder and more normal-looking Achilles tendon tissue (Fig. 6E). The Achilles tendon tissue from both sides of the rabbits was excised, and TEM revealed that the newly formed collagen fibers in the defect group were disorganized and thinner in diameter, with no apparent thick collagen fibers. In the SA group, newly formed collagen fibers were arranged in a more orderly manner; however, they were still thinner and lacked thick collagen fibers. Collagen fibers in the DPH and GDF5@DPH groups were arranged in an orderly manner, with an increasing number of thicker collagen fibers. The collagen fibers in the GDF5@DPH + TSPC group were arranged in an orderly manner, with thicker collagen fibers, and the distribution of their diameter frequency was closer to that of normal Achilles tendon tissue (Fig. 6F-M). The mechanical properties of the Achilles tendon tissue from each group were examined using a tensile machine. Compared with the control and other experimental groups, the GDF5@DPH + TSPCs group had higher modulus (MPa), failure force (N), and stress at failure (MPa) values, which were more similar to those of normal Achilles tendon tissue at 6 weeks (Fig. 6O-Q).

Six weeks postoperatively, the Achilles tendons in each group were histologically evaluated by H&E staining. The defect and SA groups still exhibited large defects at the site of injury, and the fiber arrangement was disordered. The DPH and GDF5@DPH groups showed a significant decrease in defect size and a slightly more organized fiber arrangement. The GDF5@DPH + TSPC group exhibited the best healing at the site of injury, with orderly fiber arrangement (Fig. 7A). Based on Masson's staining results, the defect and SA groups still had large defects at the site of injury, with a small number of new collagen fibers and a disordered arrangement. The DPH and GDF5@DPH groups showed a significant decrease in defect size, an increase in the number of new collagen fibers, and a slightly more organized arrangement. The GDF5@DPH + TSPC group had a higher number of new collagen fibers at the site of injury, arranged in an orderly fashion (Fig. 7B). Sirius Red staining revealed that the defect and SA groups had fewer new collagen fibers and a disordered arrangement, and the ratio of type I collagen fibers to type III collagen fibers was lower than that of type III fibers. The DPH and GDF5@DPH groups showed an increase in the number of new collagen fibers, a gradually more organized arrangement, and an increase in the ratio of type I to type III collagen fibers. The GDF5@DPH + TSPC group had a higher number of new collagen fibers at the site of injury, arranged in an orderly fashion. The ratio of type I to type III collagen fibers was significantly higher (Fig. 7C). According to the semi-quantitative analysis, the GDF5@DPH + TSPC group had a significantly lower histological score (Fig. 7D) and a higher proportion of collagen fiber area (Fig. 7E) than the control and other experimental groups.

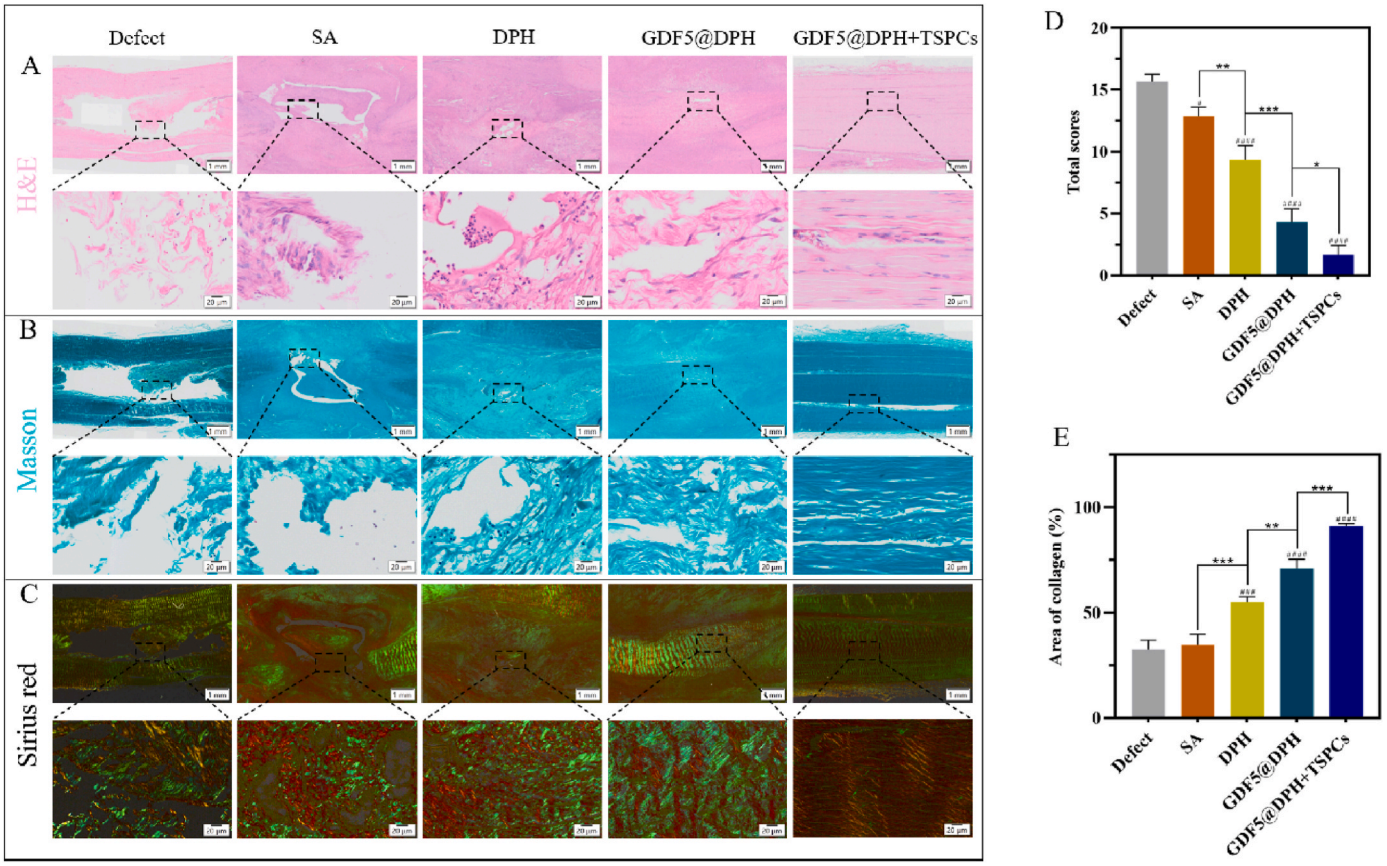

Fig. 7. Histological analysis of the Achilles tendon after operation. (A) H&E staining of the Achilles tendon tissues in each group. (B) Masson staining of the Achilles tendon tissues. (C) Sirius red staining of the Achilles tendon tissues. (D) Correlative histological scores and collagen area analysis. Data are presented as the mean ± standard deviation. n = 3 for each group, ns: not significant, # indicates comparison with SA group, $^{\#}P < 0.05$, $^{\#\#\#}P < 0.001$, $^{\#\#\#\#}P < 0.0001$, $^{*}P < 0.05$, $^{**}P < 0.01$, $^{***}P < 0.001$. Scale bars: 20 μm and 1 mm. H&E, hematoxylin and eosin. (For interpretation of the references to colour in this figure legend, the reader is referred to the Web version of this article.)

3.6. GDF5@DPH inhibits inflammatory response in Achilles tendon tissue

Achilles tendon tissues were subjected to H&E staining to assess morphological changes. In the defect group, irregular defects were observed at the center of the tendon, with remaining necrotic tendon tissue (Fig. 8A–C). In the SA group, the tendon was swollen, and the central defect was repaired through abundant granulation tissue proliferation, fibroblast proliferation, and collagen deposition. Inflammatory cells were present within the granulation tissue and transformed into scar tissue with interlaced collagen fibers. Foreign giant cells were also detected (Fig. 8D–F). In the DPH group, the tendon was swollen, and the central defect showed granulation tissue formation. Undegraded hydrogel material was scattered within the defect, accompanied by the infiltration of foreign body macrophages and inflammatory cells. Some granulation tissue had transformed into scar tissue (Fig. 8G–I). In the GDF5@DPH group, the tendon was swollen, and the central defect showed granulation tissue proliferation, extensive fibroblast proliferation, and collagen deposition. Some capillaries were observed, and most of the hydrogel material was degraded and mixed with proliferating collagen. The granulation tissue transformed into scar tissue with a relatively organized collagen fiber arrangement and a decrease in inflammatory cells (Fig. 8J-L). In the GDF5@DPH + TSPC group, a small number of irregular defects was observed, while the rest of the tendon exhibited dense connective tissue comprising abundant fibroblasts and collagen fibers without the infiltration of inflammatory cells (Fig. 8M – O). Based on quantitative analysis, the GDF5@DPH and GDF5@DPH +

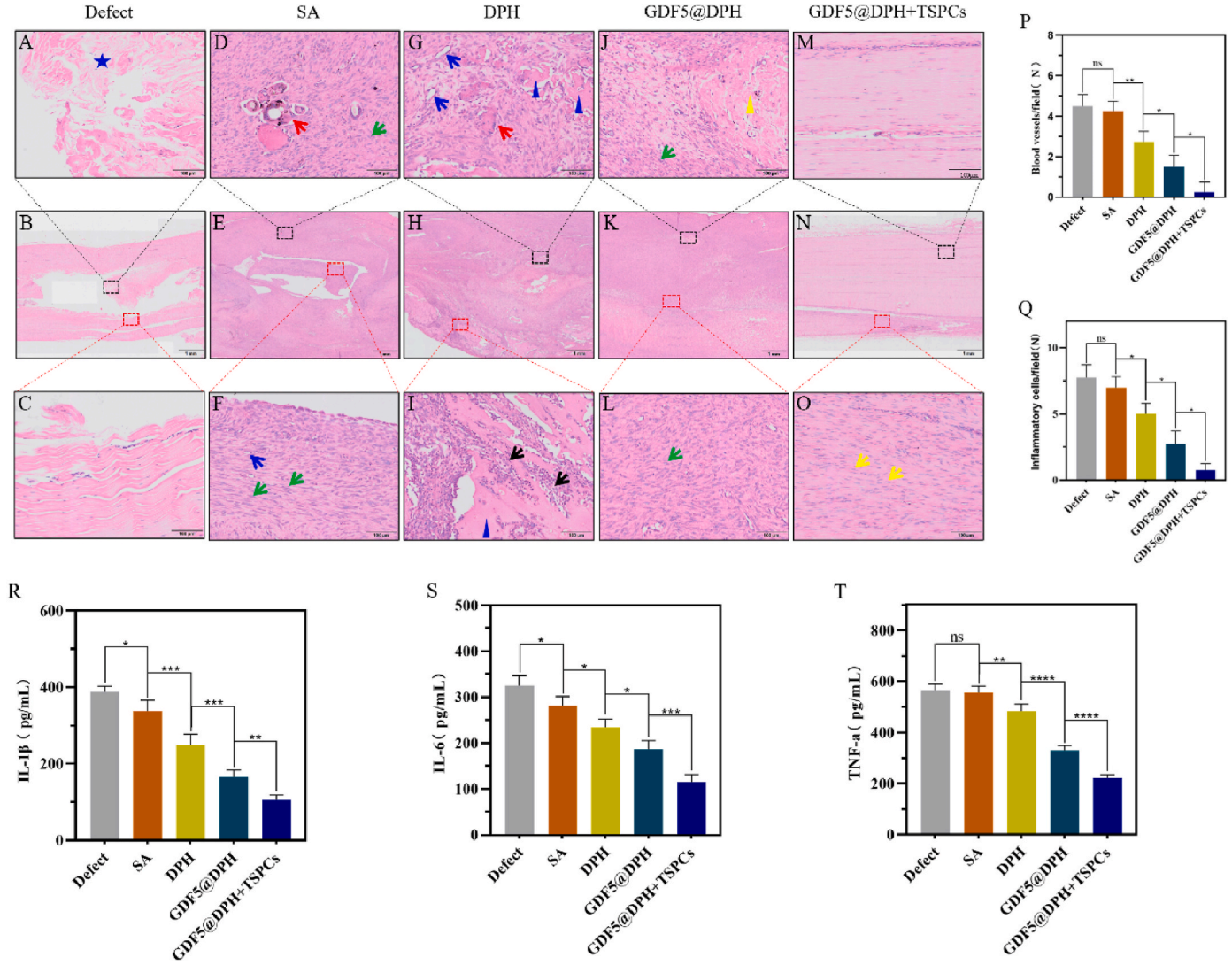

Fig. 8. Cytomorphological analysis of the Achilles tendon tissue post-surgery. (A–C) Defect group: Irregular defects can be seen in the center of the tendon, with residual tendon necrosis in the middle (blue star). (D–F) SA group: Tendon swelling and central defect repair by a large amount of granulation tissue proliferation can be observed, along with the proliferation of a large number of fibroblasts (green arrow) and collagen deposition, a small number of capillaries (blue arrow), a large number of inflammatory cells (black arrow), granulation tissue transforming into scar tissue, scar tissue collagen fibers arranged in a staggered manner, and foreign giant cells (red arrowhead). (G–I) DPH group: Tendon swelling and central defect repair by granulation tissue proliferation can be observed, along with scattered undegraded water-like gel material (blue triangle), foreign body macrophages, and inflammatory cell infiltration (black arrow), and part of the granulation tissue transformed into scar tissue. (J–L) GDF5@DPH Group: Tendon swelling, granulation tissue proliferation, and repaired central defect can be observed, along with a large number of proliferated fibroblasts and collagen deposition. The group exhibits a small number of capillaries, with most of the water-like gel material degraded, a small amount of water-like gel mixed with hypertrophic collagen (yellow triangle), granulation tissue transformed into scar tissue, neatly arranged collagen fibers, and a reduced number of inflammatory cells. (M–O) GDF5@DPH + TSCP groups: Few irregular defects can be observed, while the remaining was dense connective tissue comprising a large number of fibroblasts (yellow arrows) and collagen fibers, without notable inflammatory cell infiltration. n = 3 for each group. TSPCs, tendon stem/progenitor cells; DPH, dipeptide hydrogel; SA, sodium alginate; GDF5, growth difference factor 5. (For interpretation of the references to colour in this figure legend, the reader is referred to the Web version of this article.)

TSPCs groups had fewer vessels and inflammatory cells than the defect and SA groups, with the most notable trend observed in the GDF5@DPH + TSPCs group (Fig. 8P-Q). ELISA was performed to detect and analyze protein levels of inflammatory mediators in the Achilles tendon tissue 2 weeks postoperatively. ELISA results revealed that the production of inflammatory mediators IL-1β, IL-6, and TNF-α was suppressed in the GDF5@DPH and GDF5@DPH + TSPCs groups when compared with that in the defect and SA groups, and the trend of low expression was most notable in GDF5@DPH + TSPCs group (Fig. 8R-T).

4. Discussion

As important tissues that connect muscles and bones in the human body, tendons are prone to injury or rupture during intense exercise and are difficult to repair after injury, seriously affecting the limb movement function of patients [54,55]. Polypeptide hydrogels are excellent macromolecular biomaterials that can mimic the extracellular matrix and provide an interface and scaffold for cell growth and different biological activities [56]. Owing to their unique biocompatibility and biodegradability, polypeptide hydrogels are increasingly used in tendon injury repair [30]. In the current study, we designed P11-4 and P11-8 peptides to synthesize self-assembled hydrogels, which were used as carriers in combination with GDF5 to observe their material properties and tendon repair-promoting effects. The experimental results indicate that DPH has the characteristics of self-assembly and injectability. Compared with SA and DPH, GDF5@DPH could significantly promote TPSC differentiation into tendons and improve the repair effect of injured tendons.

The self-assembling and injectable properties of hydrogels have notable advantages in tendon injury treatment and enable the material to enter the body in a liquid state by injection, thereby avoiding other complicated reaction steps of physical crosslinking and chemical crosslinking and markedly reducing the complexity of clinical operation [57]. The injection mode of this material can reduce trauma and the risk of infection and lead to a relatively short recovery period. Herein, we synthesized DPHs using the P11-4 and P11-8 peptides. We found that the bi-polypeptides bind to each other through hydrophobic bonds, π–π bonds, and electrostatic interactions and form β-sheet structures. The DPH was injectable and could form gels at 37 °C, pH 7.0 in 7–8 min. Different GDF5 concentrations did not modify the gelling characteristics notably, which is beneficial for clinical application. Zhang et al. [58] synthesized a hydrogel by the self-assembly of the polypeptide Jelleine-1 (J-1), which was used to treat intestinal wall defects. The J-1 hydrogel showed injectable characteristics and could be used for 3D printing, exhibiting superior antibacterial, hemostatic, anti-adhesion, and other functions. Vilchez et al. [59] synthesized functional hydrogels for wound hemostasis via the self-assembly of fibrinogen and Fmoc-FF and Fmoc-FF polypeptides. The authors found that the composite hydrogel exhibited injectable characteristics and excellent hemostatic functions. Tanmay et al. [27] synthesized a composite hydrogel using amino acids/peptides. The hydrogel also showed excellent injectability during the experiment, was used as a delivery vehicle for anticancer drugs, and was not affected by the external environment. Consistently, the DPH synthesized in the current study had the same gel-forming characteristics as those observed previously, indicating that DPH is an excellent tendon repair material. Its self-assembly and injectable characteristics make it easy to quantitatively and accurately inject into the injured site, which cannot be achieved using conventional oral or intravenous injection methods.

Collagen is an important component of tendons, and peptides are components of collagen. Polypeptide hydrogels are usually composed of short peptide sequences, have good biocompatibility and degradability, can form stable 3D structures *in vivo*, provide a supporting and guiding environment, and promote cell attachment and proliferation. The advantage of this hydrogel is that it provides a microenvironment similar to the natural matrix for cells, eliciting the necessary physical support and chemical signals, thus making it an ideal tendon repair material [60]. Herein, we found the DPH has better hydrophilicity than the traditional SA hydrogel. SEM analysis revealed that the material had a higher void ratio and larger pore size, and the structure was conducive to the adhesion and growth of tendon stem cells on its surface. CCK8 and fluorescence staining showed that tendon stem cells proliferated in the dipeptide hydrogel group, and cell viability was enhanced. These results indicate that the DPH exhibits better biocompatibility, and the addition of GDF5 improved its biocompatibility, which was more conducive to improving the viability of tendon stem cells. In addition, the DPH showed better material degradation, and *in vitro* degradation experiments revealed that DPH and GDF5@DPH degraded after 35 days, whereas the SA degradation rate was poor. *In vivo* animal experiments showed that 6 weeks after hydrogel injection, the DPH and GDF5@DPH groups had less hydrogel residue in the Achilles tendon than the SA group, along with reduced inflammatory cell infiltration when compared with the SA group; this was beneficial for fibrin growth and repair during tendon regeneration, and obstruction by implanted materials and foreign body reactions could be avoided. Several previous studies have also shown that polypeptide hydrogels have good biocompatibility and degradability, which are beneficial for cell proliferation and extracellular matrix production, accompanied by positive effects on inducing cell migration [22,28]. Yang et al. [61] designed and synthesized a PAA-RGD polypeptide hydrogel. The authors found that PAA-RGD polypeptide hydrogel had suitable biodegradability, excellent biocompatibility, and low immunogenicity, which are beneficial for the proliferation and migration of rabbit bone marrow mesenchymal stem cells and promote the repair of rabbit osteochondral tissue. Zhu et al. [62] promoted the growth, proliferation, and secretion of extracellular matrix and cytokines in bone marrow stem cells by adding a polypeptide hydrogel based on traditional PCL scaffolds to improve the hydrophilicity and biocompatibility, thereby facilitating the repair of bone defects. Yin et al. [30] designed and synthesized a RADA peptide hydrogel with good biocompatibility, which promoted the proliferation of tendon stem cells and inhibited cell aging. In conclusion, polypeptide hydrogels exhibit good biocompatibility and degradability, which are beneficial for cell adhesion and growth and promote tissue repair.

GDF5 plays an important role in the proliferation and differentiation of stem cells in organisms, promoting tendon tissue repair [63–65]. In the present study, we found that the GDF5@DPH group exhibited a strong ability to promote tendon differentiation of TSPCs *in vitro* when compared with the SA and DPH groups. Similarly, *in vivo*, GDF5@DPH showed better tendon repair ability than SA and DPH. These findings could be primarily attributed to the release of GDF5 from GDF5@DPH, compared with SA and pure DPH, which can induce the aggregation and tendon differentiation of endogenous TSPCs, promoting the regeneration and repair of injured tendons. Furthermore, the *in vivo* experiments revealed that the GDF5@DPH + TSPCs group exhibited a greater ability to promote tendon differentiation and tendon repair in TSPCs than the other groups. This is mainly because the tendon is a poorly cellular tissue. Compared with the endogenous recruitment of TSPCs for defect repair, the addition of exogenous TSPCs can substantially increase the number of stem cells in the damaged area and improve the efficiency of tendon repair. Additionally, we observed that the number of inflammatory cells in the defect repair area and surrounding areas was significantly reduced in the GDF@DPH and GDF5@DPH + TSPC groups when compared with that in other groups, indicating that GDF5 may play a role in reducing the inflammatory response, which is beneficial for the repair of the defect area, promoting the growth of collagen fibers, inhibiting scar formation, and preventing adhesion to surrounding tissues. Chen et al. [66] induced adipose-derived stem cells to differentiate into tendons through GDF-5 and combined them with nanoyarn scaffolds to promote the regeneration and repair of rabbit tendons. Qu et al. [67] found that GDF-5 can enhance the expression of tendon regulatory proteins by promoting P38 phosphorylation in mouse mesenchymal stem cells, which contributes to tendon regeneration and repair. Burcu

et al. [68] found that the SF/P3HB scaffold facilitates the proliferation and differentiation of rodent-derived adipose-derived mesenchymal stem cells into tendon cells; however, the addition of GDF5 did not substantially impact cell differentiation. This could be attributed to the antibacterial effect of the scaffold, which may affect the differentiation of tendon stem cells. Different concentrations of GDF5 also play a role in stem cell differentiation. Herein, we found that the GDF5 concentration may not be the optimal concentration for promoting tendon stem cell differentiation. Fitzgerald et al. [42] found that adipose-derived stem cells cultured with GDF5 and platelet-derived growth factor could improve the healing of rat tendons after transverse injury. Haslund et al. [69] found that lower doses of GDF-5 more effectively inhibited adhesion and did not adversely impact the strength of tendon repair in mice, indicating that GDF5 also exerts a certain degree of anti-fibrotic effect. These findings are consistent with our experimental results, indicating that GDF5 plays an important role in promoting stem cell tendon differentiation and repair. In the current study, combining GDF5 with a dipeptide hydrogel was more conducive to the growth and differentiation of tendon stem cells in the defect area and improved the regeneration and repair efficiency of damaged tendons.

In conclusion, we used an injectable self-assembled dipeptide hydrogel containing GDF5 as a novel therapeutic strategy to promote the repair of damaged tendons. Based on our experimental results, the hydrogel demonstrates good biocompatibility, markedly enhances the differentiation of TSPCs into tendons, allows injection into different injury sites quantitatively and accurately, improves the regeneration and repair efficiency of injured tendons, prevents tissue adhesion, and avoids the risks associated with surgery and the series of sequelae. Compared with other studies, our study provides a more effective, feasible, and safe treatment method with a high potential for clinical application.

Although this study revealed some interesting results, the limitations need to be addressed. First, this study utilized animal models, not patients with tendon injury; therefore, we cannot directly generalize our results to humans. Although animal models are widely used in the early stages of research, there are still differences between these models and the human condition, such as differences in tendon structure and metabolic pathways, which may lead to different physiological responses. Therefore, further studies are required to verify the applicability of these findings in humans. Second, the sample size was relatively small, and the reliability of the findings may be limited. Future studies should expand the sample size to increase the reliability and representativeness of the results.

5. Conclusion

Our results showed that DPH had good injectability and biocompatibility, and GDF5@DPH promoted the proliferation and tendonogenic differentiation of TSPCs, as well as facilitated the regeneration and repair of tendon cells and collagen fibers in injured areas. Simultaneously, GDF5@DPH can inhibit inflammatory reactions in tissues, provide a favorable internal environment for tendon repair, and prevent tissue adhesion and scar hyperplasia. Therefore, the formulated injectable self-assembled DPH containing GDF5 is a feasible and effective new method for treating tendon injury and warrants further investigation and application.

Funding

This study was supported by the National Natural Science Foundation of China (No. 81871812) and the Natural Science Foundation of Jiangsu Province (BK20221462).

CRediT authorship contribution statement

Ming Zhang: Writing – original draft, Validation, Data curation, Conceptualization. **Hao Wang:** Software, Formal analysis. **Guan-Chun Dai:** Software, Formal analysis. **Pan-Pan Lu:** Software, Methodology. **Yu-Cheng Gao:** Software, Methodology. **Mu-Ming Cao:** Methodology, Investigation. **Ying-Juan Li:** Methodology, Investigation. **Yun-Feng Rui:** Writing – review & editing, Resources, Funding acquisition, Conceptualization.

Declaration of competing interest

The authors declare that they have no known competing financial interests or personal relationships that could have appeared to influence the work reported in this paper.

Data availability

Data will be made available on request.

Acknowledgments

We would like to thank Editage (www.editage.cn) for English language editing.

Appendix A. Supplementary data

Supplementary data to this article can be found online at https://doi.org/10.1016/j.mtbio.2024.101046.

References

[1] C.M. King, M. Vartivarian, Achilles tendon rupture repair: simple to complex, Clin. Podiatr. Med. Surg. 40 (1) (2023) 75–96, https://doi.org/10.1016/j.cpm.2022.07.006.
[2] V. Citro, M. Clerici, A.R. Boccaccini, G. Della Porta, N. Maffulli, N.R. Forsyth, Tendon tissue engineering: an overview of biologics to promote tendon healing and repair, J. Tissue Eng. 14 (2023) 20417314231196275, https://doi.org/10.1177/20417314231196275.
[3] B. Liaghat, J.R. Pedersen, R.S. Husted, L.L. Pedersen, K. Thorborg, C.B. Juhl, Diagnosis, prevention and treatment of common shoulder injuries in sport: grading the evidence - a statement paper commissioned by the Danish Society of Sports Physical Therapy (DSSF), Br. J. Sports Med. 57 (7) (2023) 408–416, https://doi.org/10.1136/bjsports-2022-105674.
[4] A.K. Hahn, C. Coladonato, J.J. Corvi, N.K. Patel, J.H. Sonnier, F. Tjoumakaris, K. B. Freedman, Outcomes and complications following chronic patellar tendon repair: a systematic review, Cureus 15 (7) (2023) e41713, https://doi.org/10.7759/cureus.41713.
[5] G. Yang, B.B. Rothrauff, R.S. Tuan, Tendon and ligament regeneration and repair: clinical relevance and developmental paradigm, Birth Defects Res C Embryo Today 99 (3) (2013) 203–222, https://doi.org/10.1002/bdrc.21041.
[6] Y. Li, W. Li, X. Liu, X. Liu, B. Zhu, S. Guo, C. Wang, D. Wang, S. Li, Z. Zhang, Effects of low-intensity pulsed ultrasound in tendon injuries, J. Ultrasound Med. 42 (9) (2023) 1923–1939, https://doi.org/10.1002/jum.16230.
[7] Z.L. Teng, S.X. Cao, X. Ma, X. Wang, J.Z. Huang, C. Zhang, X. Geng, Epidemiological characteristics of patients operated for achilles tendon rupture in Shanghai, Orthop. Surg. 14 (8) (2022) 1649–1655, https://doi.org/10.1111/os.13347.
[8] A.Z. Khan, K.E. Stoll, B.J. Erickson, Rehabilitation and return to work and sport after rotator cuff, Clin. Sports Med. 42 (1) (2023) 175–184, https://doi.org/10.1016/j.csm.2022.08.008.
[9] C. Fryar, D. Tilley, E. Casey, H. Vincent, A research and clinical framework for understanding achilles injury in female collegiate gymnasts, Curr. Sports Med. Rep. 22 (7) (2023) 260–267, https://doi.org/10.1249/JSR.0000000000001082.
[10] D. Seow, W. Islam, G.W. Randall, M.T. Azam, M.L. Duenes, J. Hui, C.J. Pearce, J. G. Kennedy, Lower re-rupture rates but higher complication rates following surgical versus conservative treatment of acute achilles tendon ruptures: a systematic review of overlapping meta-analyses, Knee Surg. Sports Traumatol. Arthrosc. 31 (8) (2023) 3528–3540, https://doi.org/10.1007/s00167-023-07411-1.
[11] R.N. Dickinson, J.E. Kuhn, Nonoperative treatment of rotator cuff tears, Phys. Med. Rehabil. Clin 34 (2) (2023) 335–355, https://doi.org/10.1016/j.pmr.2022.12.002.
[12] B.K. Gundlach, D.S. Zelouf, Flexor tendon reconstruction, Hand Clin. 39 (2) (2023) 193–201, https://doi.org/10.1016/j.hcl.2022.08.020.
[13] J. Chen, C. Jiang, L. Yin, Y. Liu, Y. He, S. Li, H. Shen, A review of the role of tendon stem cells in tendon-bone regeneration, Med Sci Monit 29 (2023) e940805, https://doi.org/10.12659/MSM.940805.
[14] H. Wang, G.C. Dai, Y.J. Li, M.H. Chen, P.P. Lu, Y.W. Zhang, M. Zhang, M.M. Cao, Y. F. Rui, Targeting senescent tendon stem/progenitor cells to prevent or treat age-

related tendon disorders, Stem Cell Rev Rep 19 (3) (2023) 680–693, https://doi.org/10.1007/s12015-022-10488-9.
[15] J. Lu, H. Chen, K. Lyu, L. Jiang, Y. Chen, L. Long, X. Wang, H. Shi, S. Li, The functions and mechanisms of tendon stem/progenitor cells in tendon healing, Stem Cell. Int. 2023 (2023) 1258024, https://doi.org/10.1155/2023/1258024.
[16] D. Quintero, C. Perucca Orfei, L.D. Kaplan, L. de Girolamo, T.M. Best, D. Kouroupis, The roles and therapeutic potentialof mesenchymal stem/stromal cells and their extracellular vesicles in tendinopathies, Front. Bioeng. Biotechnol. 11 (2023) 1040762, https://doi.org/10.3389/fbioe.2023.1040762.
[17] L.L. Hsiao, R.J. Howard, M. Aikawa, T.F. Taraschi, Modification of host cell membrane lipid composition by the intra-erythrocytic human malaria parasite Plasmodium falciparum, Biochem. J. 274 (Pt 1) (1991) 121–132, https://doi.org/10.1042/bj2740121.
[18] J. Zhang, J.H. Wang, Characterization of differential properties of rabbit tendon stem cells and tenocytes, BMC Muscoskel. Disord. 11 (2010) 10, https://doi.org/10.1186/1471-2474-11-10.
[19] R. Binaymotlagh, L. Chronopoulou, C. Palocci, Peptide-based hydrogels: template materials for tissue engineering, J. Funct. Biomater. 14 (4) (2023), https://doi.org/10.3390/jfb14040233.
[20] N. Kulkarni, P. Rao, G.S. Jadhav, B. Kulkarni, N. Kanakavalli, S. Kirad, S. Salunke, V. Tanpure, B. Sahu, Emerging role of injectable dipeptide hydrogels in biomedical applications, ACS Omega 8 (4) (2023) 3551–3570, https://doi.org/10.1021/acsomega.2c05601.
[21] S. Ma, S. Gu, J. Zhang, W. Qi, Z. Lin, W. Zhai, J. Zhan, Q. Li, Y. Cai, Y. Lu, Robust drug bioavailability and safety for rheumatoid arthritis therapy using D-amino acids-based supramolecular hydrogels, Mater Today Bio 15 (2022) 100296, https://doi.org/10.1016/j.mtbio.2022.100296.
[22] S.J. Jones, A. Perez, Molecular modeling of self-assembling peptides, ACS Appl. Bio Mater. (2023), https://doi.org/10.1021/acsabm.2c00921.
[23] Y. Tian, L. Lu, Recent advances in self-assembling peptide matrices as functional coatings for implantable devices, Front. Chem. 10 (2022) 1040499, https://doi.org/10.3389/fchem.2022.1040499.
[24] L. Tan, R. Huan, L.F. Wu, Y. Bao, Y.C. Ma, Q.L. Zou, J. Yong, Peptide-based nanomaterials: self-assembly and applications, Mini Rev. Med. Chem. 23 (4) (2023) 399–411, https://doi.org/10.2174/1389557522666220819103907.
[25] C.B.P. Oliveira, V. Gomes, P.M.T. Ferreira, J.A. Martins, P.J. Jervis, Peptide-based supramolecular hydrogels as drug delivery agents: recent advances, Gels 8 (11) (2022), https://doi.org/10.3390/gels8110706.
[26] X. Yao, Y. Hu, M. Lin, K. Peng, P. Wang, Y. Gao, X. Gao, T. Guo, X. Zhang, H. Zhou, Self-assembling peptide RADA16: a promising scaffold for tissue engineering and regenerative medicine, Nanomedicine (Lond) (2023), https://doi.org/10.2217/nnm-2023-0161.
[27] R. Li, Q.L. Zhou, M.R. Tai, K. Ashton-Mourney, M.I. Harty, A. Rifai, C.L. Parish, D. R. Nisbet, S.Y. Zhong, R.J. Williams, Simple complexity: incorporating bioinspired delivery machinery within self-assembled peptide biogels, Gels 9 (3) (2023), https://doi.org/10.3390/gels9030199.
[28] S. Yang, C. Wang, J. Zhu, C. Lu, H. Li, F. Chen, J. Lu, Z. Zhang, X. Yan, H. Zhao, X. Sun, L. Zhao, J. Liang, Y. Wang, J. Peng, X. Wang, Self-assembling peptide hydrogels functionalized with LN- and BDNF- mimicking epitopes synergistically enhance peripheral nerve regeneration, Theranostics 10 (18) (2020) 8227–8249, https://doi.org/10.7150/thno.44276.
[29] Y. Zhao, L. Song, M. Li, H. Peng, X. Qiu, Y. Li, B. Zhu, C. Liu, S. Ren, L. Miao, Injectable CNPs/DMP1-loaded self-assembly hydrogel regulating inflammation of dental pulp stem cells for dentin regeneration, Mater Today Bio 24 (2024) 100907, https://doi.org/10.1016/j.mtbio.2023.100907.
[30] H. Yin, F. Strunz, Z. Yan, J. Lu, C. Brochhausen, S. Kiderlen, H. Clausen-Schaumann, X. Wang, M.E. Gomes, V. Alt, D. Docheva, Three-dimensional self-assembling nanofiber matrix rejuvenates aged/degenerative human tendon stem/progenitor cells, Biomaterials 236 (2020) 119802, https://doi.org/10.1016/j.biomaterials.2020.119802.
[31] A. Imere, C. Ligorio, M. O'Brien, J.K.F. Wong, M. Domingos, S.H. Cartmell, Engineering a cell-hydrogel-fibre composite to mimic the structure and function of the tendon synovial sheath, Acta Biomater. 119 (2021) 140–154, https://doi.org/10.1016/j.actbio.2020.11.017.
[32] K. Fu, H. Wu, Z. Su, Self-assembling peptide-based hydrogels: fabrication, properties, and applications, Biotechnol. Adv. 49 (2021) 107752, https://doi.org/10.1016/j.biotechadv.2021.107752.
[33] P. Rozhin, S. Adorinni, D. Iglesias, T. Mackiol, S. Kralj, M. Bisetto, M. Abrami, M. Grassi, M. Bevilacqua, P. Fornasiero, S. Marchesan, Nanocomposite hydrogels with self-assembling peptide-functionalized carbon nanostructures, Chemistry (2023) e202301708, https://doi.org/10.1002/chem.202301708.
[34] M. Lin, W. Li, X. Ni, Y. Sui, H. Li, X. Chen, Y. Lu, M. Jiang, C. Wang, Growth factors in the treatment of Achilles tendon injury, Front. Bioeng. Biotechnol. 11 (2023) 1250533, https://doi.org/10.3389/fbioe.2023.1250533.
[35] S. Wu, B. Duan, A. Lu, Y. Wang, Q. Ye, L. Zhang, Biocompatible chitin/carbon nanotubes composite hydrogels as neuronal growth substrates, Carbohydr. Polym. 174 (2017) 830–840, https://doi.org/10.1016/j.carbpol.2017.06.101.
[36] Q. Wang, L. Zhang, Z. Sun, B. Chi, A. Zou, L. Mao, X. Xiong, J. Jiang, L. Sun, W. Zhu, Y. Ji, HIF-1alpha overexpression in mesenchymal stem cell-derived exosome-encapsulated arginine-glycine-aspartate (RGD) hydrogels boost therapeutic efficacy of cardiac repair after myocardial infarction, Mater Today Bio 12 (2021) 100171, https://doi.org/10.1016/j.mtbio.2021.100171.
[37] X. Zhao, R. Bian, F. Wang, Y. Wang, X. Li, Y. Guo, X. Zhang, G. Luo, R. Zhan, GDF-5 promotes epidermal stem cells proliferation via Foxg1-cyclin D1 signaling, Stem Cell Res. Ther. 12 (1) (2021) 42, https://doi.org/10.1186/s13287-020-02106-7.
[38] L. He, S. Lan, Q. Cheng, Z. Luo, X. Lin, Self-assembling peptide SCIBIOIII hydrogel for three-dimensional cell culture that promotes wound healing in diabetic mice, Gels 9 (4) (2023), https://doi.org/10.3390/gels9040265.
[39] J. Anantha, S.R. Goulding, S.L. Wyatt, R.M. Concannon, L.M. Collins, A. M. Sullivan, G.W. O'Keeffe, STRAP and NME1 mediate the neurite growth-promoting effects of the neurotrophic factor GDF5, iScience 23 (9) (2020) 101457, https://doi.org/10.1016/j.isci.2020.101457.
[40] K. Sun, J. Guo, X. Yao, Z. Guo, F. Guo, Growth differentiation factor 5 in cartilage and osteoarthritis: a possible therapeutic candidate, Cell Prolif. 54 (3) (2021) e12998, https://doi.org/10.1111/cpr.12998.
[41] W. He, X. Lin, LINC00313 promotes the proliferation and inhibits the apoptosis of chondrocytes via regulating miR-525-5p/GDF5 axis, J. Orthop. Surg. Res. 18 (1) (2023) 137, https://doi.org/10.1186/s13018-023-03610-1.
[42] M.J. Fitzgerald, T. Mustapich, H. Liang, C.G. Larsen, K.W. Nellans, D.A. Grande, Tendon transection healing can Be improved with adipose-derived stem cells cultured with growth differentiation factor 5 and platelet-derived growth factor, Hand (N Y) 18 (3) (2023) 436–445, https://doi.org/10.1177/15589447211028929.
[43] Y. Hagiwara, F. Dyrna, A.F. Kuntz, D.J. Adams, N.A. Dyment, Cells from a GDF5 origin produce zonal tendon-to-bone attachments following anterior cruciate ligament reconstruction, Ann. N. Y. Acad. Sci. 1460 (1) (2020) 57–67, https://doi.org/10.1111/nyas.14250.
[44] A.A. de Aro, G.D. Carneiro, L.F.R. Teodoro, F.C. da Veiga, D.L. Ferrucci, G. F. Simoes, P.W. Simoes, L.E. Alvares, A.L.R. de Oliveira, C.P. Vicente, C.P. Gomes, J.B. Pesquero, M.A.M. Esquisatto, B. de Campos Vidal, E.R. Pimentel, Injured achilles tendons treated with adipose-derived stem cells transplantation and GDF-5, Cells 7 (9) (2018), https://doi.org/10.3390/cells7090127.
[45] F. Koch, M. Muller, F. Konig, N. Meyer, J. Gattlen, U. Pieles, K. Peters, B. Kreikemeyer, S. Mathes, S. Saxer, Mechanical characteristics of beta sheet-forming peptide hydrogels are dependent on peptide sequence, concentration and buffer composition, R. Soc. Open Sci. 5 (3) (2018) 171562, https://doi.org/10.1098/rsos.171562.
[46] A. Barco, E. Ingham, J. Fisher, H. Fermor, R.P.W. Davies, On the design and efficacy assessment of self-assembling peptide-based hydrogel-glycosaminoglycan mixtures for potential repair of early stage cartilage degeneration, J. Pept. Sci. 24 (8–9) (2018) e3114, https://doi.org/10.1002/psc.3114.
[47] A. Prakash, S.J. Parsons, S. Kyle, M.J. McPherson, Recombinant production of self-assembling beta-structured peptides using SUMO as a fusion partner, Microb. Cell Factories 11 (2012) 92, https://doi.org/10.1186/1475-2859-11-92.
[48] V.A.M. Gonzaga, A.L. Poli, J.S. Gabriel, D.Y. Tezuka, T.A. Valdes, A. Leitao, C. F. Rodero, T.M. Bauab, M. Chorilli, C.C. Schmitt, Chitosan-laponite nanocomposite scaffolds for wound dressing application, J. Biomed. Mater. Res. B Appl. Biomater. 108 (4) (2020) 1388–1397, https://doi.org/10.1002/jbm.b.34487.
[49] Z. Cao, H. Wang, J. Chen, Y. Zhang, Q. Mo, P. Zhang, M. Wang, H. Liu, X. Bao, Y. Sun, W. Zhang, Q. Yao, Silk-based hydrogel incorporated with metal-organic framework nanozymes for enhanced osteochondral regeneration, Bioact. Mater. 20 (2023) 221–242, https://doi.org/10.1016/j.bioactmat.2022.05.025.
[50] X. Chen, B. Tan, S. Wang, R. Tang, Z. Bao, G. Chen, S. Chen, W. Tang, Z. Wang, C. Long, W.W. Lu, D. Yang, L. Bian, S. Peng, Rationally designed protein cross-linked hydrogel for bone regeneration via synergistic release of magnesium and zinc ions, Biomaterials 274 (2021) 120895, https://doi.org/10.1016/j.biomaterials.2021.120895.
[51] L. Zhao, Q. Ding, J. Zeng, F.R. Wang, J. Zhang, S.J. Fan, X.Q. He, An improved CTAB-ammonium acetate method for total RNA isolation from cotton, Phytochem. Anal. 23 (6) (2012) 647–650, https://doi.org/10.1002/pca.2368.
[52] I. Komatsu, J.H. Wang, K. Iwasaki, T. Shimizu, T. Okano, The effect of tendon stem/progenitor cell (TSC) sheet on the early tendon healing in a rat Achilles tendon injury model, Acta Biomater. 42 (2016) 136–146, https://doi.org/10.1016/j.actbio.2016.06.026.
[53] M. Ni, P.P. Lui, Y.F. Rui, Y.W. Lee, Y.W. Lee, Q. Tan, Y.M. Wong, S.K. Kong, P. M. Lau, G. Li, K.M. Chan, Tendon-derived stem cells (TDSCs) promote tendon repair in a rat patellar tendon window defect model, J. Orthop. Res. 30 (4) (2012) 613–619, https://doi.org/10.1002/jor.21559.
[54] A. Giri, D. O'Hanlon, N.B. Jain, Risk factors for rotator cuff disease: a systematic review and meta-analysis of diabetes, hypertension, and hyperlipidemia, Ann Phys Rehabil Med 66 (1) (2023) 101631, https://doi.org/10.1016/j.rehab.2022.101631.
[55] O. Leino, H. Keskinen, I. Laaksonen, K. Makela, E. Loyttyniemi, E. Ekman, Incidence and treatment trends of achilles tendon ruptures in Finland: a nationwide study, Orthop J Sports Med 10 (11) (2022) 23259671221131536, https://doi.org/10.1177/23259671221131536.
[56] R. Pugliese, F. Gelain, Cross-linked self-assembling peptides and their post-assembly functionalization via one-pot and in situ gelation system, Int. J. Mol. Sci. 21 (12) (2020), https://doi.org/10.3390/ijms21124261.
[57] A. GhavamiNejad, N. Ashammakhi, X.Y. Wu, A. Khademhosseini, Crosslinking strategies for 3D bioprinting of polymeric hydrogels, Small 16 (35) (2020) e2002931, https://doi.org/10.1002/smll.202002931.
[58] H. Zhang, Z. Wu, J. Zhou, Z. Wang, C. Yang, P. Wang, M.S. Fareed, Y. He, J. Su, R. Cha, K. Wang, The antimicrobial, hemostatic, and anti-adhesion effects of a peptide hydrogel constructed by the all-d-enantiomer of antimicrobial peptide jelleine-1, Adv. Healthcare Mater. 12 (29) (2023) e2301612, https://doi.org/10.1002/adhm.202301612.
[59] C. Gila-Vilchez, M.C. Manas-Torres, O.D. Garcia-Garcia, A. Escribano-Huesca, L. Rodriguez-Arco, V. Carriel, I. Rodriguez, M. Alaminos, M.T. Lopez-Lopez, L. Alvarez de Cienfuegos, Biocompatible short-peptides fibrin Co-assembled

hydrogels, ACS Appl. Polym. Mater. 5 (3) (2023) 2154–2165, https://doi.org/10.1021/acsapm.2c02164.
[60] J. Zhang, D. Zhao, K. Lu, Mechanisms and influencing factors of peptide hydrogel formation and biomedicine applications of hydrogels, Soft Matter 19 (39) (2023) 7479–7493, https://doi.org/10.1039/d3sm01057k.
[61] M. Yang, Z.C. Zhang, F.Z. Yuan, R.H. Deng, X. Yan, F.B. Mao, Y.R. Chen, H. Lu, J. K. Yu, An immunomodulatory polypeptide hydrogel for osteochondral defect repair, Bioact. Mater. 19 (2023) 678–689, https://doi.org/10.1016/j.bioactmat.2022.05.008.
[62] T. Wu, Y. Wu, Z. Cao, L. Zhao, J. Lv, J. Li, Y. Xu, P. Zhang, X. Liu, Y. Sun, M. Cheng, K. Tang, X. Jiang, C. Ling, Q. Yao, Y. Zhu, Cell-free and cytokine-free self-assembling peptide hydrogel-polycaprolactone composite scaffolds for segmental bone defects, Biomater. Sci. 11 (3) (2023) 840–853, https://doi.org/10.1039/d2bm01609e.
[63] M. Govoni, A.C. Berardi, C. Muscari, R. Campardelli, F. Bonafe, C. Guarnieri, E. Reverchon, E. Giordano, N. Maffulli, G. Della Porta, (*) an engineered multiphase three-dimensional microenvironment to ensure the controlled delivery of cyclic strain and human growth differentiation factor 5 for the tenogenic commitment of human bone marrow mesenchymal stem cells, Tissue Eng Part A 23 (15–16) (2017) 811–822, https://doi.org/10.1089/ten.TEA.2016.0407.
[64] K. Vuornos, M. Bjorninen, E. Talvitie, K. Paakinaho, M. Kellomaki, H. Huhtala, S. Miettinen, R. Seppanen-Kaijansinkko, S. Haimi, Human adipose stem cells differentiated on braided polylactide scaffolds is a potential approach for tendon tissue engineering, Tissue Eng Part A 22 (5–6) (2016) 513–523, https://doi.org/10.1089/ten.tea.2015.0276.
[65] C. Holladay, S.A. Abbah, C. O'Dowd, A. Pandit, D.I. Zeugolis, Preferential tendon stem cell response to growth factor supplementation, J Tissue Eng Regen Med 10 (9) (2016) 783–798, https://doi.org/10.1002/term.1852.
[66] S. Chen, J. Wang, Y. Chen, X. Mo, C. Fan, Tenogenic adipose-derived stem cell sheets with nanoyarn scaffolds for tendon regeneration, Mater Sci Eng C Mater Biol Appl 119 (2021) 111506, https://doi.org/10.1016/j.msec.2020.111506.
[67] Y. Qu, L. Zhou, B. Lv, C. Wang, P. Li, Growth differentiation factor-5 induces tenomodulin expression via phosphorylation of p38 and promotes viability of murine mesenchymal stem cells from compact bone, Mol Med Rep 17 (3) (2018) 3640–3646, https://doi.org/10.3892/mmr.2017.8325.
[68] B. Sarikaya, M. Gumusderelioglu, Aligned silk fibroin/poly-3-hydroxybutyrate nanofibrous scaffolds seeded with adipose-derived stem cells for tendon tissue engineering, Int J Biol Macromol 193 (Pt A) (2021) 276–286, https://doi.org/10.1016/j.ijbiomac.2021.10.104.
[69] S. Hasslund, T. Dadali, M. Ulrich-Vinther, K. Soballe, E.M. Schwarz, H.A. Awad, Freeze-dried allograft-mediated gene or protein delivery of growth and differentiation factor 5 reduces reconstructed murine flexor tendon adhesions, J Tissue Eng 5 (2014) 2041731414528736, https://doi.org/10.1177/2041731414528736.